Swarm intelligence optimization of the group method of data handling using the cuckoo search and whale optimization algorithms to model and predict landslides

Abolfazl Jaafari [1,*], Mahdi Panahi [2, 3], Davood Mafi-Gholami [4], Omid Rahmati [5], Himan Shahabi [6,7], Ataollah Shirzadi [8], Changwook Lee[2] ,Saro Lee [2, 9,*], Dieu Tien Bui [10*], Biswajeet Pradhan[11,12]

1. Research Institute of Forests and Rangelands, Agricultural Research, Education and Extension Organization (AREEO), Tehran, Iran. Email: jaafari@rifr-ac.ir
2. Division of Science Education, Kangwon National University, Chuncheon-si, Gangwon-do 24341, Korea. Email: Mahdi.panahi@kigam.re.kr
3. Geoscience Platform Research Division, Korea Institute of Geoscience and Mineral Resources (KIGAM), 124, Gwahak-ro Yuseong-gu, Daejeon 34132, Korea
4. Department of Forest Sciences, Faculty of Natural Resources and Earth Sciences, Shahrekord University, Shahrekord, Iran. E-mail: d.mafigholami@nres.sku.ac.ir
5. Kordestan Agricultural and Natural Resources Research and Education Center, Agricultural Research, Education, and Extension Organization (AREEO), Sanandaj, Iran. Email: o.rahmati@areeo.ac.ir
6. Department of Geomorphology, Faculty of Natural Resources, University of Kurdistan, Sanandaj 66177-15175, Iran; h.shahabi@uok.ac.ir
7. Board Member of Department of Zrebar Lake Environmental Research, Kurdistan Studies Institute, University of Kurdistan, Sanandaj 66177-15175, Iran
8. Department of Rangeland and Watershed Management, Faculty of Natural Resources, University of Kurdistan, Sanandaj 66177-15175, Iran; a.shirzadi@uok.ac.ir
9. Department of Geophysical Exploration, Korea University of Science and Technology, 217 Gajeong-ro, Yuseong-gu, Daejeon 34113, Korea. E-mail: leesaro@kigam.re.kr
10. Institute of Research and Development, Duy Tan University, Da Nang 550000, Viet Nam. E-mail: buitiendieu@duytan.edu.vn
11. Centre for Advanced Modelling and Geospatial Information Systems (CAMGIS), Faculty of Engineering and Information Technology, University of Technology Sydney, New South Wales, Australia. E-mail: Biswajeet.Pradhan@uts.edu.au
12. Department of Energy and Mineral Resources Engineering, Sejong University, Choongmu-gwan, 209 Neungdong-ro Gwangjin-gu, Seoul 05006, Korea

* Corresponding authors: jaafari@rifr-ac.ir (A. Jaafari), leesaro@kigam.re.kr (S. Lee), and buitiendieu@duytan.edu.vn (D.T. Bui)

Abstract

The development of powerful and robust landslide predictive models has become a major focus among landslide researchers. This paper proposes two novel hybrid predictive models that combine the self-organizing deep-learning group method of data handling (GMDH) and two swarm intelligence optimization algorithms, i.e., cuckoo search algorithm (CSA) and whale optimization algorithm (WOA) for of the prediction landslide susceptibility in a spatially explicit manner. Eleven causative factors and 334 historic landslides from a 31,340 km^2 landslide-prone area in Iran were used to produce the training and validation datasets required for the building and validation of the models. The GMDH model was utilized to develop a basic predictive model that was then restructured and optimized using the CSA and WOA algorithms, yielding two novel hybrid GMDH-CSA and GMDH-WOA models. The hybrid models that profited from an intelligent approach to overcome the computational shortcomings of the base GMDH model demonstrated a statistically significant improvement in generalization and predictive abilities by up to 9.5 and 13%, respectively. Further, the hybrid models demonstrated higher robustness in comparison with the single GMDH model, as they consistently depicted excellent performance when the training and validation datasets altered. Overall, our study indicates that swarm intelligence optimized models can identify optimal trade-offs between objectives, accuracy, and robustness, which would otherwise not have been possible using single simple models.

Keywords: Landslide susceptibility, GMDH, Whale optimization algorithm, Cuckoo search algorithm, GIS, Iran.

1. Introduction

Landslides are among the deadliest and costliest natural disasters that cause significant losses of lives (Guzzetti et al., 1999; Wood et al., 2020) and global economic damages of over billion dollars (Haque et al., 2019; Highland and Bobrowsky, 2008). The large proportion of personal property and infrastructure that reside in areas susceptible to landslides is a subject of particular concern (Dao et al., 2020; Jaafari et al., 2019a) that have placed strong demands on authorities and engineers to delimit the landscapes in terms of susceptibility to landslide occurrences (Fallah-Zazuli et al., 2019). Identifying areas with high landslide susceptibility must be undertaken to ensure the continued sustainable growth of human infrastructure. Landslide susceptibility mapping provides authorities and managers with reliable information for making more informed land use and development decisions for the landslide-prone areas (Jaafari et al., 2015b; Nefeslioglu and Gorum, 2020).

The first extensive works on landslide susceptibility mapping and modeling date back to Brabb et al. (1972) in the USA and Carrara and Merenda (1976) in Italy (Jaafari et al., 2019a; Van Westen et al., 2008). To date, landslide susceptibility has been modeled based on a variety of statistical, knowledge based, and machine learning methods. The choice of each method is usually related to the balance of the availability of dada, accuracy requirement, modelers' ability, and computational resources (Bragagnolo et al., 2020a; Dao et al., 2020; Jaafari et al., 2019a; Jessee et al., 2020; Moayedi et al., 2019a; Moayedi et al., 2019c; Pourghasemi and Rahmati, 2018; Shafizadeh-Moghadam et al., 2019).

While the statistical- and knowledge-based methods offer the easiest and most commonly employed approaches for landslide susceptibility mapping (Jaafari et al., 2014; Thanh et al., 2020), their application is limited by some prior assumptions such as the normal distribution of data and input variables must be conditionally independent of one another (Jaafari et al., 2017). In contrast, machine learning methods make no initial assumptions about the data and allow for direct information extraction from the phenomenon being modeled (Dao et al., 2020; Pham et al., 2019).

However, the performance of machine learning methods can further be improved through using hybrid ensemble modeling approaches (Jaafari et al., 2019b; Jaafari et al., 2019c; Moayedi et al., 2019e; Nhu et al., 2020; Rahmati et al., 2019b). In the domain of landslide prediction, efforts have been made to develop hybrid ensemble models through three main methodological approaches: (1) feeding a method by the output of another method (e.g., weight of evidence and analytic hierarchy process (Jaafari, 2018)), (2) employing ensemble learning techniques for manipulating the input dataset for a base method (e.g., bagging, boosting, and stacking with support vector machine (SVM) (Dou et al., 2019)), and (3) employing meta-heuristic optimization algorithms for tuning the hyper-parameters of a method (e.g., biogeography-based optimization and artificial neural network (ANN) (Moayedi et al., 2019d)). All these three approaches have been proven to be effective for providing more accurate and reliable estimates of landslide susceptibilities than the standalone simple methods. Among them, the third approach has become an active research area in recent years. Starting with the pioneering works of Bui et al. (2017), Chen et al. (2017), Bui et al. (2018), and Jaafari et al. (2019a), the application of meta-heuristic optimization algorithms has recently emerged as a prominent approach for the development of meta-optimized landslide predictive models. Various hybrid predictive models in the form of combinations of the SVM, ANN, adaptive neuro-fuzzy inference system extreme (ANFIS), and learning machines (ELM) with the different meta-heuristic optimization algorithms (e.g., genetic algorithm (GA), particle swarm optimization (PSO), differential evolution (DE), dragonfly algorithm (DA), biogeography-based optimization (BBO), grey wolf optimizer (GWO), ant colony optimization (ACO), artificial bee colony (ABC), and Harris hawks optimization (HHO)) have been suggested to improve the prediction of landslides (Bui et al., 2019; Chen et al., 2019a; Chen et al., 2019b; Jaafari et al., 2019a; Moayedi et al., 2019a; Nguyen et al., 2019a; Nguyen et al., 2019b; Tien Bui et al., 2019; Xi et al., 2019).

In spite of the widespread application of machine learning methods for the prediction of landslides, many other methods that have not yet been investigated for their capability to predict landslide susceptibility. Group method of data handling (GMDH) is a self-organizing algorithm from the deep learning ANNs family that has been designed for solving the problem of modeling multi-input to standalone-output data. This method is a self-organizing modeling approach because the number of layers and their neurons and the characteristics of the produced neurons are automatically adjusted during a self-organization process. GMDH has a history of successful applications for energy and environment, engineering, industrial processes, telecommunications, biomedicine, and education (Gascón-Moreno et al., 2013). However, GMDH has not yet been used for landslide susceptibility modeling and mapping. Therefore, this study was conducted (1) to develop spatially-explicit predictive models based on the GMDH method, (2) to determine whether the hybrid models based on the GMDH method and meta-heuristic optimization algorithms achieve greater accuracy for the prediction of landslide susceptibilities compared to the standalone GMDH model, and (3) to evaluate which optimization algorithms (i.e., cuckoo search algorithm (CSA) and whale optimization algorithm (WOA)) can most improve GMDH for landslide prediction.

We used the information of historical landslides collected from a landslide-prone region in the northwest of Iran and corresponding data related to topography, climate, and human activity that has been previously suggested for developing landslide prediction models. By developing a new hybrid predictive model and its application in a yet unstudied landslide-prone area, this study contributes to increasing the general knowledge on the capability of different machine learning methods for the prediction of landslides which in turn enables authorities and manager to adopt cost-effective resilience-based management strategies.

2. Study area

For this study, a landslide-prone area from the northwest of Iran was selected (Fig. 1). This area consists of the whole territory of the Ardabil Province and some parts of the Azarbaijan Sharghi, Guilan, and Zanjan provinces of Iran. This region covers a total area of 31,340 km^2 and is located between 36° 32′ to 39° 42′ N latitude and 47° 00′ to 49° 36′ E longitude (Fig. 1). The area has a diverse and rugged topography, including hills, valleys, and coastal areas. The hilly and mountainous terrains (elevation = -107─4783 m; slope degree = 0─88) cover the central and western portions of the area, accounting for 76% of the land area. The range of hills and mountains gradually decreases towards the coastal areas of the Caspian Sea with an average slope of 6 degree and elevation of 180 m. Range lands, forests, farmlands, orchards, and residential areas are the primary land uses in the research area. The meteorological data from the period of 1988─2017 shows that the mean annual rainfall varies between 222 mm in the north part and 1900 mm in the southeastern part of the area, with an average of 480 mm. This area is subjected to frequent landslides such that the global view of landslide susceptibility (EOS, 2017) shows a moderate-to-severe landslide potential for this area. Incidence and magnify the severity of landslides in this area have been amplified due to extensive and unplanned human activities in the recent years.

3. Modeling steps

The steps to complete modeling of landslide susceptibility using the hybrid intelligence models based on the GMDH method include: (1) detecting historical landslides and non-landslide locations across the study area, (2) mapping potential landslide causative factors, (3) exploring spatial relationships between historical landslides and causative factors, (4) developing hybrid intelligence predictive models, (5) robustness analysis via five-fold cross-validation, (6) producing surface maps of landslide susceptibilities, and (7) quantitative evaluation of the predictive models and susceptibility maps (Fig. 2).

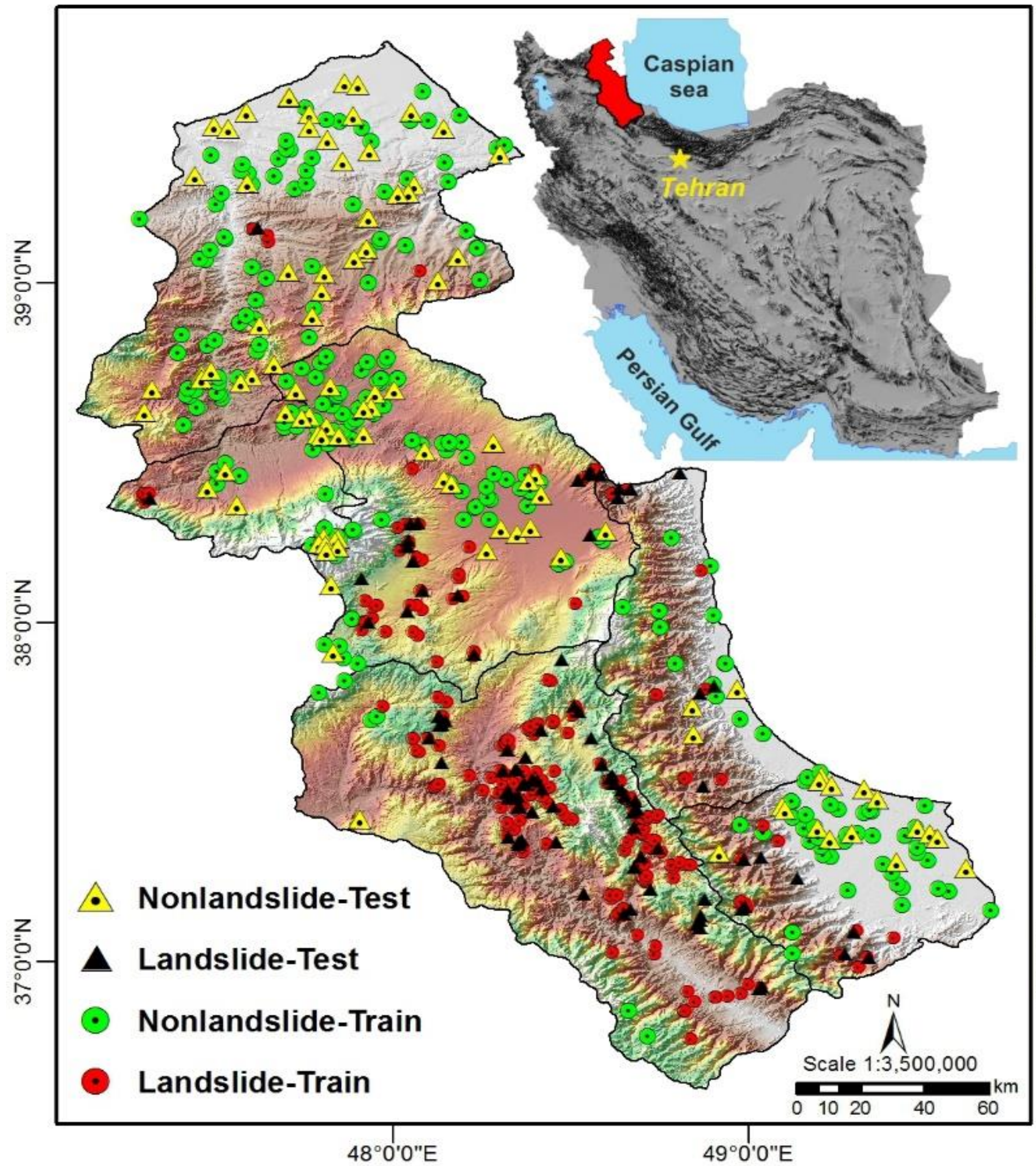

Fig. 1. Location map of the study area with the landslide inventories.

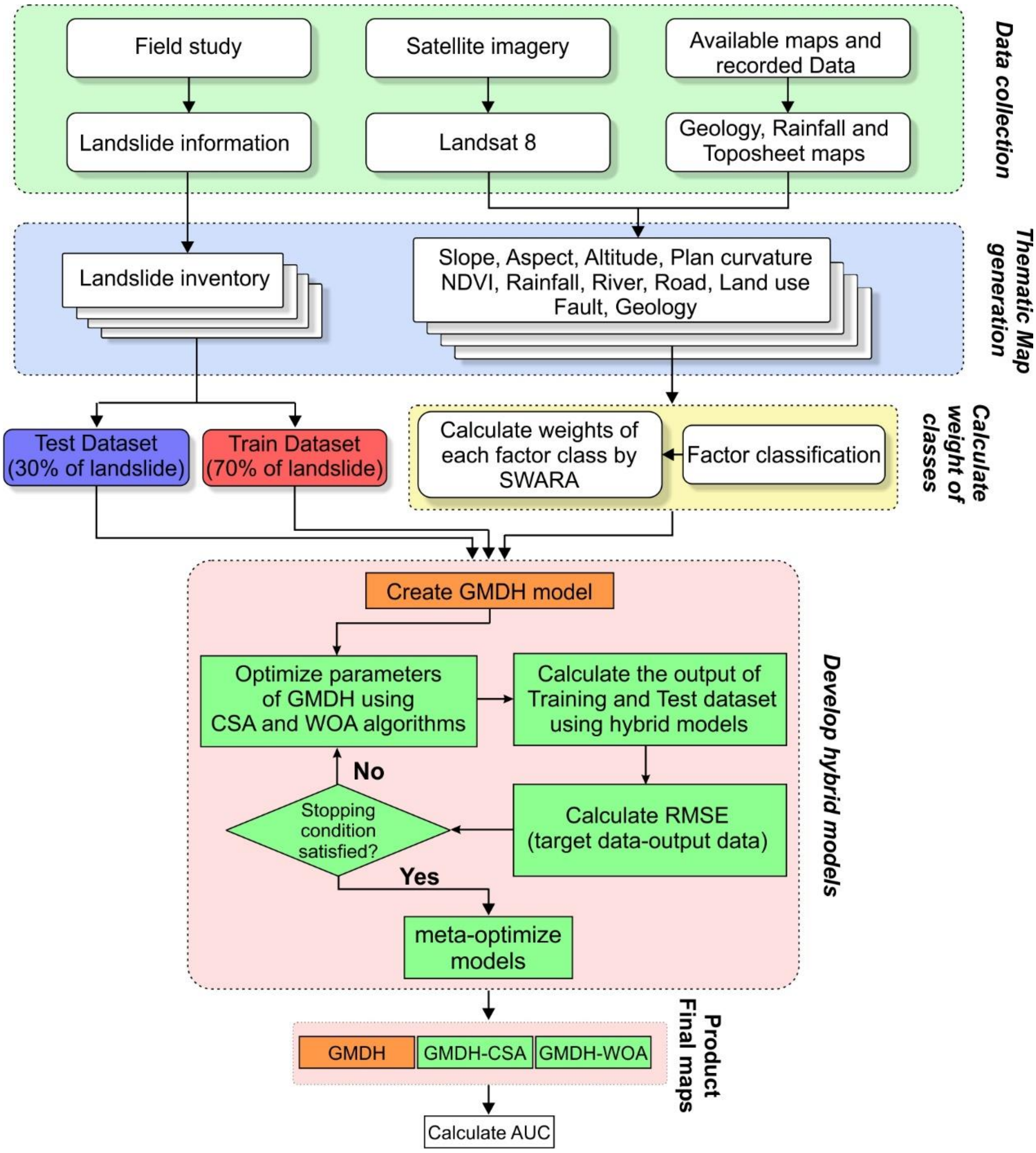

Fig. 2. Flowchart of model development for landslide susceptibility mapping.

3.1. Construction of the geospatial database

3.1.1. Landslide inventory

Information on the past landslides that have happened in the study region was collected to generate an inventory map. Information on the landslides occurred before the year 2015 was obtained from the Forests, Range and Watershed Management Organization of Iran. For landslides that have occurred in the period between 2015 and 2018, the information was obtained from local authorities. Lastly, for recent landslides, the information was obtained from the field surveys and observations. This information includes the type and spatial location of each landslide that revealed that rock fall events, soil slides, and debris flows were the dominant types of landslides in this portion of the country. The ultimate inventory map encompassed 334 landslide locations. Along with the landslide locations, we sampled 334 locations as non-landslide locations from the areas without any evidence of landslide occurrences. Landslide and non-landslide locations were merged and randomly divided into independent sets. The first set encompassed 70% of data (234 landslides and 234 non-landslides), which was selected as the training dataset, and the second set involved the remaining data (100 landslides and 100 non-landslides), which was used as the validation dataset (Fig. 1).

3.1.2. Landslide causative factors

Various topographical, geomorphological, and environmental factors influence the probability of landslide occurrences. In spatially-explicit landslide modeling, these factors are independent/explanatory variables that are typically selected based on the availability of data objective and scale of the analysis. In this study, we selected eleven factors: elevation (m), slope (degree), aspect, curvature, rainfall (mm), land use, normalized difference vegetation index (NDVI), geology, and distance to roads, rivers, and faults.

Given the strong correlation between topography features and landslides (Bragagnolo et al., 2020a; Chen et al., 2019a; Dao et al., 2020; Jaafari, 2018; Moayedi et al., 2019e; Tien Bui et al., 2019), four main topographic features that have been recurrently used for landslide modeling (slope, aspect, altitude, and curvature) were also used in this study. We employed an ASTER Digital Elevation Model (DEM) with 30 m resolution (https://vertex.daac.asf.alaska.edu) to generate the maps of topographic features for the study area (Fig. 3a-d). To generate an annual rainfall map for the study area, 30-year data (1988-

2017) from 32 metrological stations over the area were interpolated using the simple kriging technique (Fig. 3e). Land-use type is frequently used as a proxy for explaining landscape modification and changing the land cover, drainage system, and runoff hydrograph due to human activities that often lead to landslide occurrences (Glade, 2003; Reichenbach et al., 2014; Shu et al., 2019). Here, we produced the land-use map of the research area using the Landsat 8 OLI satellite images via the maximum likelihood classification technique that exhibited a variety of land-use types across the landscape (Fig. 3f). NDVI quantifies land cover by distinguishing between near-infrared and red wavelengths. We used this index as a landslide causative factor because many previous studies demonstrated a relationship between land covers and landslides, with lower vegetation density indicating higher probability of landside occurrences (Glade, 2003; Jaafari et al., 2014; Jaafari et al., 2015a; Jaafari et al., 2015b; Machado et al., 2019). Here, we produced the NDVI map of the study area (Fig. 3g) using the Landsat 8 OLI satellite images (Mafi-Gholami et al., 2020; Mafi-Gholami et al., 2019). Proximity variables (distance to roads, rivers, and faults) are important landslide causative factors because the landslide activities generally change within different distances from roads, rivers, and faults (Gorum and Carranza, 2015; Larsen and Montgomery, 2012; Schlögl and Matulla, 2018). The proximity maps were generated using the Euclidian distance tool in ArcGIS 10.3 (Fig. 3h-j). The geology that characterizes soil and underlying rock types and affects the erosion process, infiltration, and runoff (Gorum et al., 2008; Van Westen et al., 2003; Vanmaercke et al., 2017) was another landslide causative factor used in this study. This map was collected from the National Cartographic Centre and Geological Survey of Iran (Fig. 3k).

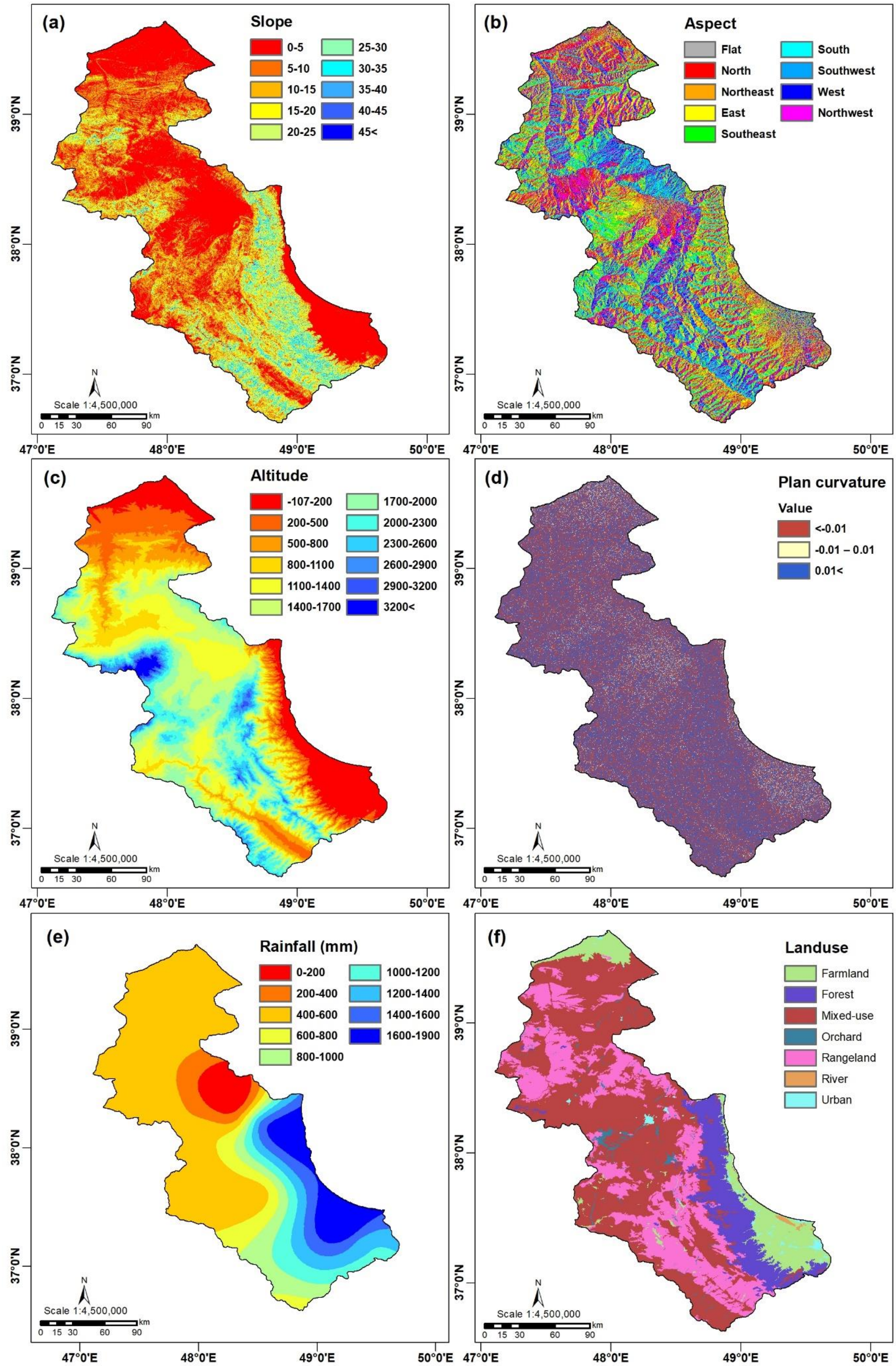
(a)
Slope
0-5
5-10
10-15
15-20
20-25
25-30
30-35
35-40
40-45
45<
(b)
Aspect
Flat
North
Northeast
East
Southeast
South
Southwest
West
Northwest
(c)
Altitude
-107-200
200-500
500-800
800-1100
1100-1400
1400-1700
1700-2000
2000-2300
2300-2600
2600-2900
2900-3200
3200<
(d)
Plan curvature
Value
<-0.01
-0.01 – 0.01
0.01<
(e)
Rainfall (mm)
0-200
200-400
400-600
600-800
800-1000
1000-1200
1200-1400
1400-1600
1600-1900
(f)
Landuse
Farmland
Forest
Mixed-use
Orchard
Rangeland
River
Urban
N
Scale 1:4,500,000
0 15 30 60 90 km
39°0'N
38°0'N
37°0'N
47°0'E
48°0'E
49°0'E
50°0'E

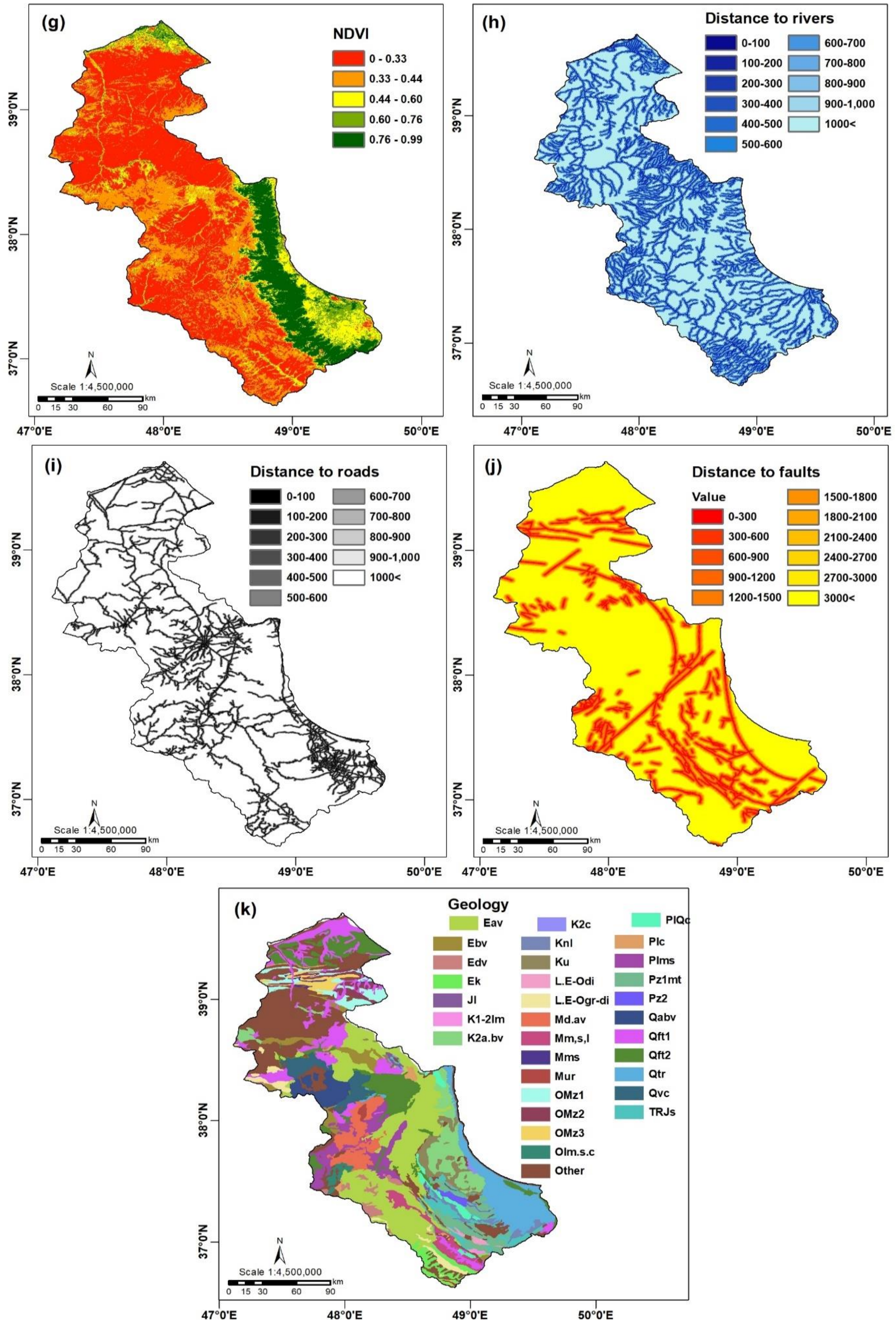

Fig. 3. Landslide causative factors used in this study.

3.2. Methods used

3.2.1. Step-wise weight assessment ratio analysis (SWARA)

To explore the spatial association between historical landslides and different causative factors with the aim of measuring the significance of each factor class on landslide occurrence, we used the step-wise weight assessment ratio analysis (SWARA) procedure. SWARA, developed by Keršuliene et al. (2010), is one of the most widely used methods for measuring factor weight in different fields of science (Zolfani and Chatterjee, 2019). Compared to other multi-criteria decision-making techniques (e.g., analytic hierarchy process (AHP) and analytic network process (ANP)) SWARA uses a simpler computational process for ranking the factors (Jaafari et al., 2015a; Jaafari et al., 2019a). To estimate the importance of each category of the landslide causative factors using the SWARA method, we prioritized the classes of a given factor based on their significance on landslide occurrences and the local condition of the study area. Then, the classes were assigned a weight such that the highest weight was given to the most important class and the lowest weight was given to the least effective class. Finally, the average ranks given by the experts was used to rank the causative factors (Jaafari et al., 2019c). Using this procedure, each class of each landslide causative factor was assigned a weight that indicates the extent of the spatial association between each class and the likelihood of landslide occurrences.

3.2.2. Group method of data handling (GMDH)

The combination of a multi-layered network in which a set of nodes and layers is produced via a number of selected input from the set of designed data being modeled is known as the GMDH algorithm. This idea of this artificial intelligence method was first articulated by Ivakhnenko (1968) for identifying nonlinear input-output relationships in the real-world problems. This method builds a generalized polynomial-based function model in a feed-forward network.

Then, the original network grows in an adaptive way to reach an optimized degree of complexity such that at the end of the process the model is neither too complex (to avoid over-fitting) nor too simple (it must be generalizable) (Fig. 4).

The significant difference between GMDH and other networks is that the GMDH network changes continuously during the training course to find the optimum structure. GMDH has been successfully applied to handle uncertainty and to deal with linear or nonlinearity systems in different fields of science (Harandizadeh et al., 2019).

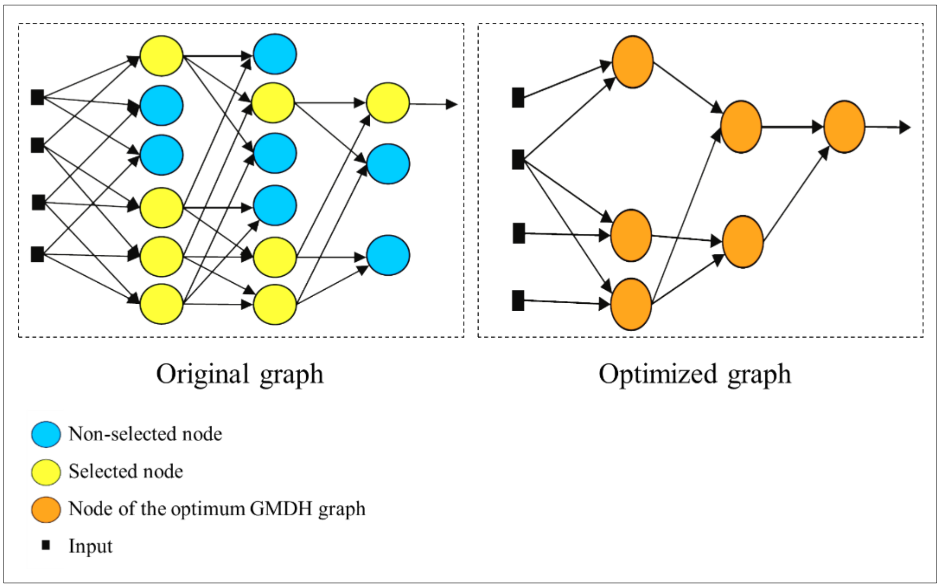

Fig. 4. GMDH network construction.

The application of GMDH for the prediction of landslide susceptibility can formally be given as follows: let $X = \{x_1, x_2, \ldots, x_n\}$ be the set of input factors (i.e., landslide causative factors) and y be the actual outputs (i.e., susceptibility indices the range between 0 to 1) such that x_j, $y \in \mathrm{R}^m$, where $j = 1, \ldots, n$. The main idea is to an approximation ($\hat{f}$) of the actual function f such that the difference between the predicted susceptibility indices and the actual susceptibility indices to be as small as possible. To archive this, the ith output can be given in terms of the inputs as follows:

$$y_i = f(x_{i1}, x_{i2}, \ldots, x_{in}) \quad (1)$$

where $i = 1, 2, . . . , m$ and x_{ij} represent the ith component of x_j .

The ith predicted output $\hat{y}_i$ is expressed by:

$$\hat{y}_i = \hat{f}(x_{i1}, x_{i2}, ..., x_{in}) \tag{2}$$

Accordingly, GMDH is used to solve the following optimization problem:

$$\min \sum_{i=1}^{m} (\hat{f}(x_{i1}, x_{i2}, ..., x_{in}) - y_i)^2 = \min_{\hat{y}} \sum_{i=1}^{m} (\hat{y}_i - y_i)^2 = \min_{\hat{y}} \|\hat{y}_i - y\|_2^2 \tag{3}$$

where $\hat{y} = (\hat{y}_1 + \hat{y}_2, ...\hat{y}_m)^T$, $y = (y_1 + y_2, ...y_m)^T$, and $\|\hat{y}_i - y\|_2^2$ is 2-norm of the vector $\hat{y} - y$. In GMDH, the general input-output relationship is built upon the Kolmogorov-Gabor polynomial function (Ivakhnenko, 1971):

$$y = w_0 \sum_{p=1}^{n} w_p x_p + \sum_{p=1}^{n} \sum_{q=1}^{n} w_{pq} x_p x_q + \sum_{p=1}^{n} \sum_{q=1}^{n} \sum_{k=1}^{n} w_{pqk} x_p x_q x_k + ... \tag{4}$$

Detailed information about the GMDH method can be found in Ivakhnenko (1971), Witczak et al. (2006), and Saberi-Movahed et al. (2020).

3.2.3. Cuckoo search algorithm (CSA)

CSA, developed by Yang and Deb (2009), is swarm-based meta-heuristic optimization algorithm that mimics the brood parasitism of some birds (e.g., *Tapera naevia*) from the cuckoo family (i.e., Cuculidae) which are unable to raise their offspring. Instead, they attempt to imitate colors and pattern of other birds' eggs (Fig. 5a, b) (Yang, 2013). The cuckoo birds drop their eggs into the host birds' nest so that the hosts raise the young cuckoos after the egg hatching. The young cuckoos quickly push the host bird's eggs to capture more food from for increasing the survival possibility (Fig. 5c). However, the host birds sometimes identify and destroy the strange eggs, otherwise abandon the nest to construct a completely new nest elsewhere (Fig. 5d). Thus, the cuckoo birds use an intelligent random strategy to select the host nest to place their eggs. This strategy is based on the by Lévy flight, which is typically used to explain many natural and artificial facts (e.g., the movement behavior of animals, fluid dynamics, earthquake analysis, cooling behavior, noise, and Ladar Scanning) (Haklı and Uğuz, 2014). In CSA, the Lévy flight is used to represent both local and global search process (Yang and Deb, 2009), which enables the algorithm to simultaneously find all possible optimum solutions in a design space. Incorporating this breeding behavior into a meta-heuristic algorithm, the CSA optimization algorithm was suggested and used for various optimization problems. In CSA, each egg is a solution to the problem (i.e., for our case is a GMDH parameter). The best sets of solution (i.e., nests with the highest quality of eggs) are passed to the next generations. With a probability of P = [0,1], the discovering operator removes the worst nest from further calculations (Sanajaoba and Fernandez, 2016). Further information of this optimization algorithm can be found in the literature (Meneses et al., 2020; Yang, 2014; Yang and Deb, 2009).

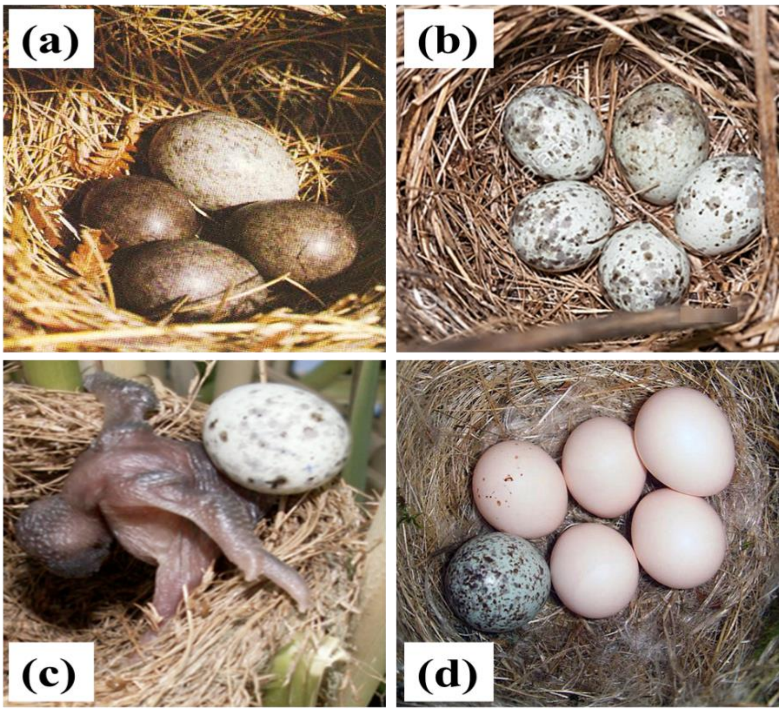

Fig. 5. Cuckoo's egg between host's eggs (a and b); cuckoo chick removes host's eggs (c); odd egg in the nest (d).

3.2.4. Whale optimization algorithm (WOA)

WOA is another swarm-based meta-heuristic optimization algorithm, first proposed by Mirjalili and Lewis (2016). WOA simulates the social intelligence of humpback whales (*Megaptera novaeangliae*) and their exceptional hunting behavior, which is called bubble-net feeding method. In this hunting behavior that is unique to humpback whales, a group of whales dive beneath the school of krill or small fishes by creating high pitch calls. Then, the prey run away to the surface, where the whales release the distinctive bubbles along a circle of the 9-shaped trail (Fig. 6) in an upward shrinking spiral around the prey as an obstacle that makes the prey unable to swim. Finally, the whales spirally swim-up with their mouths open to get the prey (Chen et al., 2019a). The mathematical modeling of WOA based on the bubble net attack consist of three main phase: 1) Exploration: this phase corresponds to whale attempts for find the prey. In this phase, position update agents are applied to find global optima. Each agent can change its location with respect to other agent, which is called shrinking encircling mechanism (Petrović et al., 2019). 2) Exploitation: when the agents find a position near global optima, the exploration phase is terminated and the exploitation phase begins. In this phase, the agents update their position in respect to the leader based on the shrinking encircling mechanism. 3) Spiral bubble-net feeding maneuver: this mode is a mixed search method, where both exploitation or exploration may happen. Full description of the WOA algorithm and its source codes are available at http://www.alimirjalili.com/WOA.html.

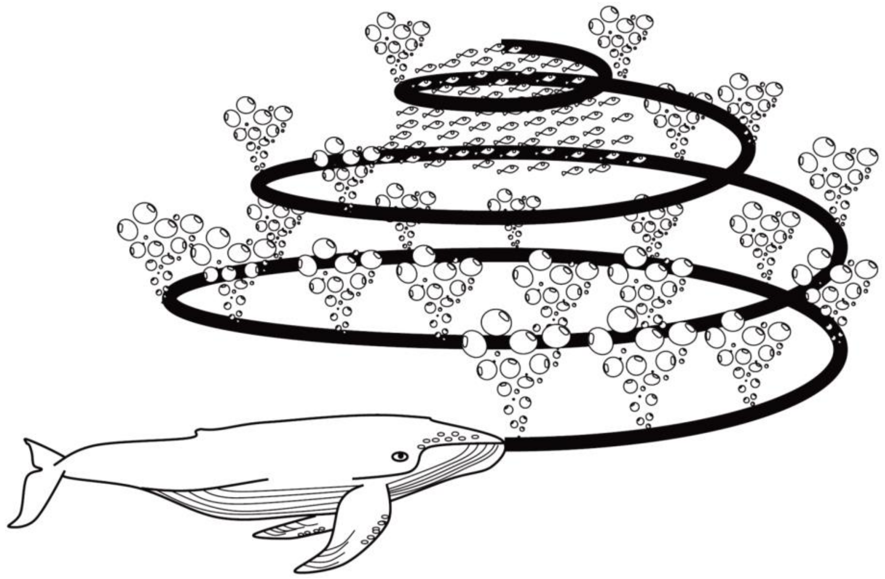

Fig. 6. Bubble-net feeding behavior of humpback whales (Mirjalili and Lewis, 2016).

3.3. Hybrid intelligence models

GMDH has several parameters (e.g., a number of nodes in each layer) that need to be properly adjusted for the best model performance. Modelers mostly tend to adjust the parameters through a trial-and-error procedure that may affect the model performance and computation time. Another drawback to the use of original GMDH is that this method is highly prone to over-fitting. This problem typically stems from improper use of the GMDH stopping criteria that cause to a model with a too complex structure. Lastly, GMDH suffers from the multi-collinearity problem that can considerably increase the average error of the GMDH method. The Multi-collinearity problem happens when the coefficients of the nodes are significantly correlated with the coefficients of different layers. Here, we elected to use the CSA and WOA to optimize the parameters of the GMDH method and to overcome the inherent drawbacks to the classical GMDH method. This approach leads to the development of two hybrid intelligence models, namely GMDH-CSA and GMDH-WOA, for the prediction of landslide susceptibility. The fitness function (i.e., stopping criteria) for these two hybrid models was the root-mean-square error (RMSE) (Eq. 5) that computes the extent of the error between the landslide/non-landslide pixels and the probability indices of future landslides, with lower RMSEs demonstrating higher predictive performance (Bennett et al., 2013; Chen et al., 2019a; Jaafari et al., 2019b; Jaafari et al., 2019c). The training process of the models consists of three main steps: adding layers to the GMDH structure, calculating the fitness function, and eliminating the neurons that decrease the quality of the results. In this procedure, the outputs of a current layer are used as the inputs for the next layer. The training course is terminated when the new layer fails to increase the overall performance of the model.

$$RMSE = \sqrt{\frac{1}{n}\sum_{i=1}^{n}(Tg_i - Op_i)^2} \quad (5)$$

where n donates the number of samples, Tg_i presents target values in the training dataset or the validation dataset, and Op_i is the output values of the predictive models.

The modeling process was coded in the MATLAB programming language on a personal laptop with an Intel(R) Core(TM) i5-4200u CPU @ 3.30 GHz, 4 GB of installed memory (RAM), a x64-based processor, and the Microsoft Windows 8.1 operating system.

3.3.1. Robustness analysis

To check for the model robustness, we used a five-fold cross-validation method by which the initial dataset was randomly divided into five sets. Out of these five sets, one set was used as the validation set and the rest were used as the training set. Then, we trained the models using the training sets and validated using the validation set. We repeated the modeling process until each one of the five sets were used as the validation set (Fig. 7).

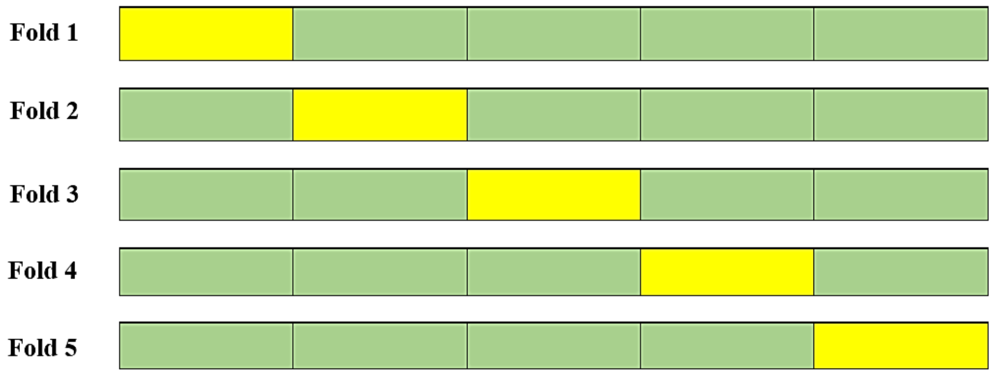

Fig. 7. Five-fold cross-validation method used in this study (in each fold, green and yellow boxes are training and validation datasets, respectively.)

3.3.2. Characterizing performance of the models

Establishment an appropriate level of confidence in performance and output is essential for reliable application of landslide predictive models. In this study, the performance of the models was validated in terms of the generalizability (i.e., goodness-of-fit with training dataset) and predictive capability. For these two levels of model performance, we first calculated the RMSE (Eq. 1) that measured the magnitude of the training and validation errors (Bennett et al., 2013). We next calculated the receiver operating characteristic curve (ROC) that measured the overall performance of the predictive models (Althuwaynee et al., 2012; Bragagnolo et al., 2020b; Du et al., 2020). The ROC method calculates the success and prediction rates to provide a trade-off between the sensitivity (i.e., false negatives; the proportion of correctly categorized landslide pixels) and 100-specificity (i.e., false positives; the proportion of correctly categorized non-landslide pixels) (Tosteson and Begg, 1988). This calculation results in the area under the curve (AUC) that ranges between 0 and 1. A value close to 1 indicates that the model performed well in separating the landslide and non-landslide pixels, whereas a value ≤ 0.5 indicates the low ability for class separation (Hanley and McNeil, 1982).

To determine if there is statistical significance between the AUC values of the success rates and between the AUC values of the prediction rates, the nonparametric Wilcoxon signed-rank test with a 95% confidence level (*p-value* < 0.05) was used (Hong et al., 2019).

4. Results and analysis

4.1. Application of the SWARA method

Applying the SWARA method, we were enabled to quantify the class importance for all the causative factors and rank their influences on landslide occurrences within the study area (Table 1). The results exhibited that the most susceptible portions of the study area to landslides have a plan curvature ≥ -0.01 ($SWARA_{weight}$ = 0.24 and 0.38), NDVI of 0.33-0.44 ($SWARA_{weight}$ = 0.28), distance to roads < 200 m ($SWARA_{weight}$ = 022), rainfall of 100-120 mm ($SWARA_{weight}$ = 0.21), elevation 1700-2000 m ($SWARA_{weight}$ = 0.21), and slope degree of 10-15 ($SWARA_{weight}$ = 0.20). In contrast, several other classes with $SWARA_{weight}$ of zero or close to zero (e.g., elevation ≥ 2900 and slope ≥ 40°) were identified as the least important factor classes on the probability of landslide occurrence.

Table 1. $SWARA_{weight}$ for each class of the landslide causative factors

Factor	Class	No. of pixels in domain	Percentage of pixels	No. of landslides	Percentage of landslides	$SWARA_{weight}$
Elevation (m)	-107 - 200	551004	12.66	8	3.43	0.04
	200-500	398896	9.16	15	6.44	0.09
	500-800	373004	8.57	10	4.29	0.07
	800-1100	411285	9.45	13	5.58	0.08
	1100-1400	719670	16.53	34	14.59	0.11
	1400-1700	713360	16.38	67	28.76	0.18
	1700-2000	545479	12.53	64	27.47	0.21
	2000-2300	337965	7.76	18	7.73	0.12
	2300-2600	173103	3.98	3	1.29	0.05
	2600-2900	77472	1.78	1	0.43	0.04
	2900-3200	23875	0.55	0	0.00	0.00
	3200<	28834	0.66	0	0.00	0.00

Slope degree	0-5	1747842	40.14	38	16.31	0.07
	5-10	803218	18.45	56	24.03	0.14
	10-15	585559	13.45	59	25.32	0.20
	15-20	442394	10.16	39	16.74	0.18
	20-25	344850	7.92	22	9.44	0.13
	25-30	251574	5.78	16	6.87	0.13
	30-35	137269	3.15	2	0.86	0.05
	35-40	35302	0.81	1	0.43	0.09
	40-45	4905	0.11	0	0.00	0.00
	45<	1034	0.02	0	0.00	0.00
Aspect	Flat (-1)	6281	0.14	0	0.00	0.01
	North	609873	14.01	29	12.45	0.11
	Northeast	618019	14.19	34	14.59	0.13
	East	613277	14.09	31	13.30	0.12
	Southeast	559783	12.86	32	13.73	0.13
	South	456782	10.49	25	10.73	0.13
	Southwest	439525	10.09	39	16.74	0.18
	West	479967	11.02	20	8.58	0.10
	Northwest	570440	13.10	23	9.87	0.10
Plan Curvature	<-0.01	2016906	46.32	112	48.07	0.39
	-0.01 – 0.01	187012	4.30	4	1.72	0.24
	0.01<	2150029	49.38	117	50.21	0.38
NDVI	0 - 0.33	289331	49.46	102	43.78	0.20
	0.33 - 0.44	150485	25.73	88	37.77	0.28
	0.44 - 0.60	47236	8.08	15	6.44	0.18
	0.60 - 0.76	36311	6.21	11	4.72	0.17
	0.76 - 0.99	61594	10.53	17	7.30	0.16
Rainfall (mm)	0-20	187619	4.31	2	0.86	0.04
	20-40	212359	4.88	5	2.15	0.06
	40-60	2084206	47.87	107	45.92	0.12
	60-80	281411	6.46	26	11.16	0.17
	80-100	327639	7.53	29	12.45	0.17
	100-120	312874	7.19	37	15.88	0.21
	120-140	312771	7.18	9	3.86	0.08
	140-160	271861	6.24	9	3.86	0.09
	160-190	363040	8.34	9	3.86	0.07
Land use	Urban	42351	0.01	6	0.01	0.20
	Orchard	56782	0.01	8	0.02	0.20
	Farmland	407576	0.09	54	0.12	0.19
	Mixed-use	2175793	0.50	267	0.57	0.17
	Rangeland	1156751	0.27	109	0.23	0.14
	Forest	492670	0.11	23	0.05	0.09
	River	11506	0.00	0	0.00	0.01
Dis. to faults (m)	0 - 300	249831	5.06	10	4.29	0.06
	300 - 600	242731	4.92	17	7.30	0.10

	600 - 900	226744	4.59	16	6.87	0.10
	900 - 1200	211710	4.29	12	5.15	0.09
	1200 - 1500	201954	4.09	15	6.44	0.11
	1500 - 1800	192368	3.90	16	6.87	0.12
	1800 - 2100	182038	3.69	13	5.58	0.11
	2100 - 2400	170617	3.45	15	6.44	0.13
	2400 - 2700	161706	3.27	8	3.43	0.08
	2700 - 3000	153182	3.10	3	1.29	0.04
	3000<	2945639	59.65	108	46.35	0.06
Dis. to rivers (m)	0 - 100	269594	5.46	15	6.44	0.09
	100 - 200	265405	5.37	21	9.01	0.13
	200 - 300	258436	5.23	22	9.44	0.14
	300 - 400	251734	5.10	14	6.01	0.09
	400 - 500	244733	4.96	17	7.30	0.11
	500 - 600	236429	4.79	11	4.72	0.08
	600 - 700	226709	4.59	9	3.86	0.07
	700 - 800	215970	4.37	4	1.72	0.04
	800 - 900	204340	4.14	13	5.58	0.10
	900 - 1000	193103	3.91	8	3.43	0.07
Dis. to roads (m)	0 - 100	210575	4.26	108	46.35	0.22
	100 - 200	198673	4.02	10	4.29	0.05
	200 - 300	185879	3.76	25	10.73	0.13
	300 - 400	174609	3.54	20	8.58	0.11
	400 - 500	164545	3.33	15	6.44	0.09
	500 - 600	155872	3.16	13	5.58	0.08
	600 - 700	147947	3.00	16	6.87	0.11
	700 - 800	141156	2.86	10	4.29	0.07
	800 - 900	134666	2.73	8	3.43	0.06
	900 - 1000	128744	2.61	4	1.72	0.04
	1000 <	3295854	66.74	4	1.72	0.02
Geology	Eav	867007	17.66	58	24.89	0.03
	Ebv	113622	2.31	2	0.86	0.01
	Edv	51967	1.06	10	4.29	0.07
	Ek	78150	1.59	2	0.86	0.01
	Jl	12188	0.25	3	1.29	0.08
	K1-2lm	4598	0.09	1	0.43	0.08
	K2a.bv	239298	4.88	7	3.00	0.01
	K2c	8853	0.18	1	0.43	0.05
	Knl	43224	0.88	3	1.29	0.03
	Ku	102422	2.09	1	0.43	0.01
	L.E-Odi	16764	0.34	1	0.43	0.03
	L.E-Ogr-di	71430	1.46	9	3.86	0.05
	Md.av	170859	3.48	16	6.87	0.04
	Mm,s,l	91379	1.86	9	3.86	0.04
	Mms	9953	0.20	1	0.43	0.04
	Mur	12746	0.26	1	0.43	0.03
	Olm.s.c	30567	0.62	1	0.43	0.02
	OMz1	111377	2.27	3	1.29	0.01
	OMz2	66658	1.36	1	0.43	0.01

OMz3	57368	1.17	1	0.43	0.01
other	842500	17.16	0	0.00	0.00
Plc	27199	0.55	2	0.86	0.03
Plms	186329	3.80	20	8.58	0.04
PlQc	56317	1.15	15	6.44	0.09
Pz1mt	148124	3.02	12	5.15	0.03
Pz2	22455	0.46	1	0.43	0.02
Qabv	113291	2.31	2	0.86	0.01
Qft1	384592	7.84	7	3.00	0.01
Qft2	406509	8.28	7	3.00	0.01
Qtr	318963	6.50	3	1.29	0.01
Qvc	127740	2.60	6	2.58	0.02
TRJs	113978	2.32	26	11.16	0.08

4.2. Model performance

The application of the predictive models determined the relationship between input variables (causative factors and historical landslides) and output (landslide susceptibilities) that revealed that the magnitude of the modeling error (RMSE) of the three models ranges from 0.088 (GMDH-CSA) to 0.224 (GMDH) in the training phase and from 0.089 (GMDH-CSA) to 0.226 (GMDH) in the validation phase (Figs 8-10). These results show that the two hybrid intelligence models achieved lower training and validation errors than the standalone GMDH model, indicating that the CSA and WOA meta-heuristic optimization algorithms performed well in optimizing the structure of the base GMDH model toward achieving higher modeling accuracy. The GMDH-CSA model that showed lower magnitude of validation error than that of the GMDH and GMDH-WOA models was identified as the most accurate hybrid model in terms of the predictive capability.

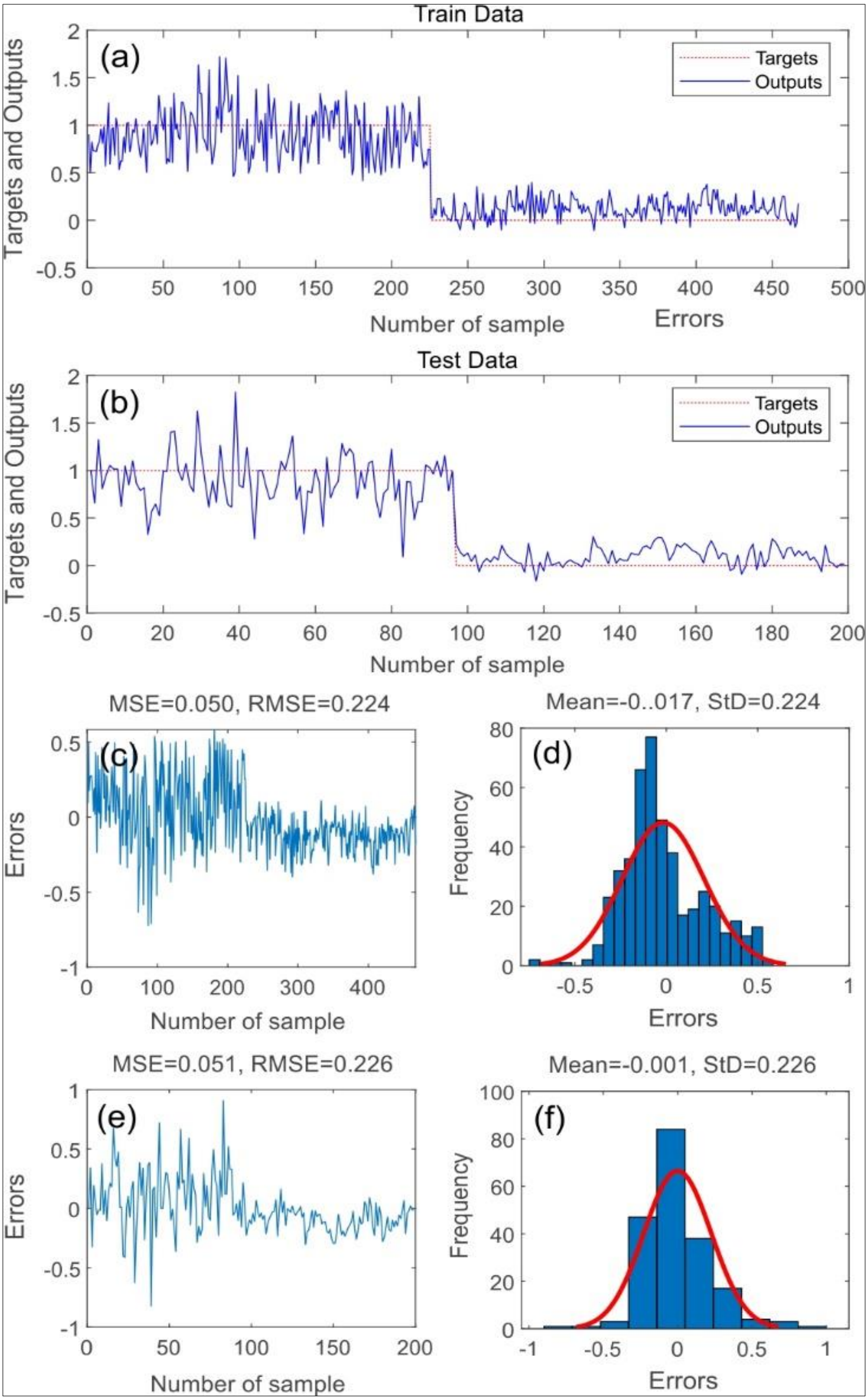

Fig. 8. GMDH performance: a) target and output values in the training phase, b) target and output values in the validation phase, c) magnitude of training error, d) distribution of training error, e) magnitude of validation error, and f) distribution of validation error.

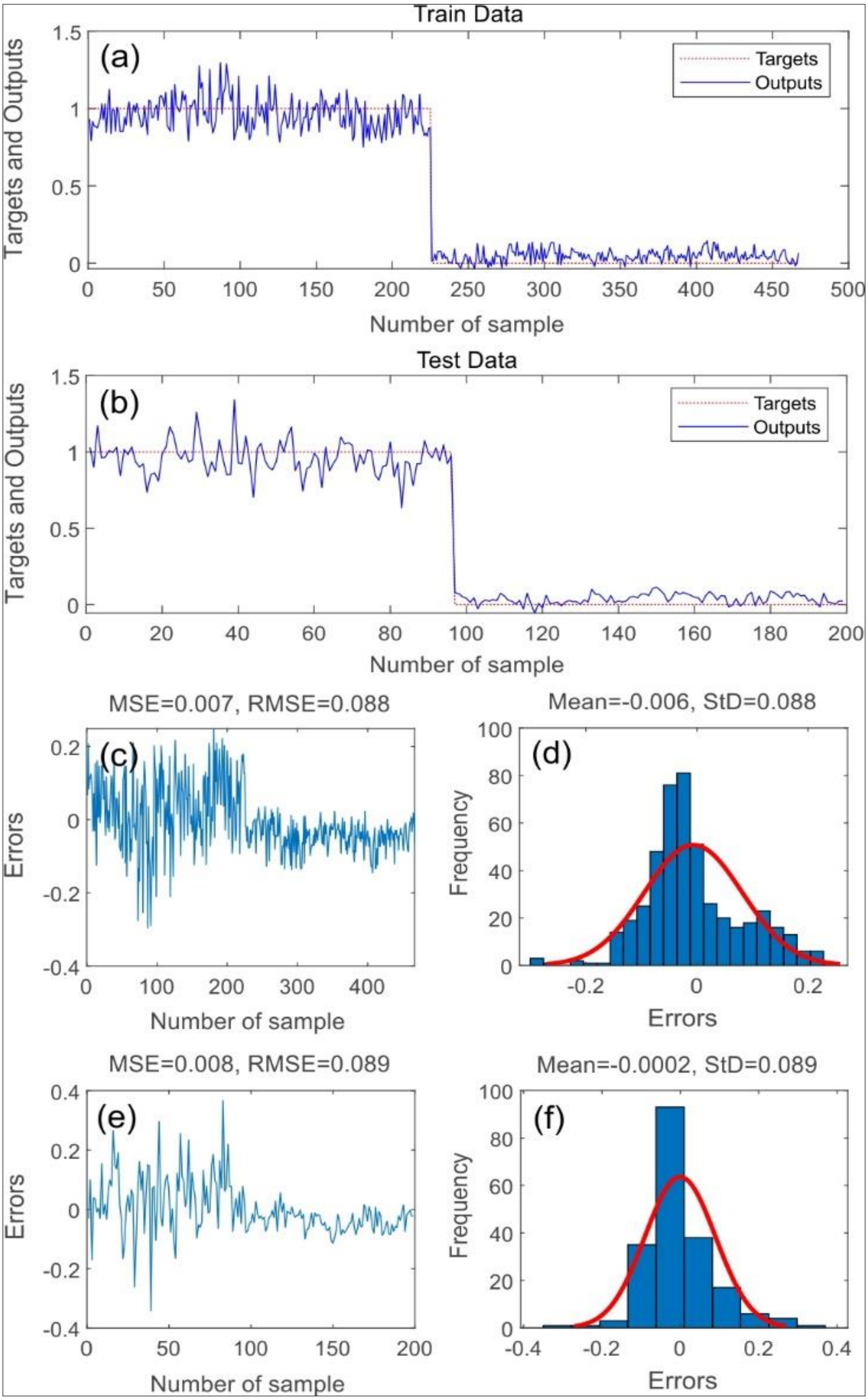

Fig. 9. GMDH-CSA performance: a) target and output values in the training phase, b) target and output values in the validation phase, c) magnitude of training error, d) distribution of training error, e) magnitude of validation error, and f) distribution of validation error.

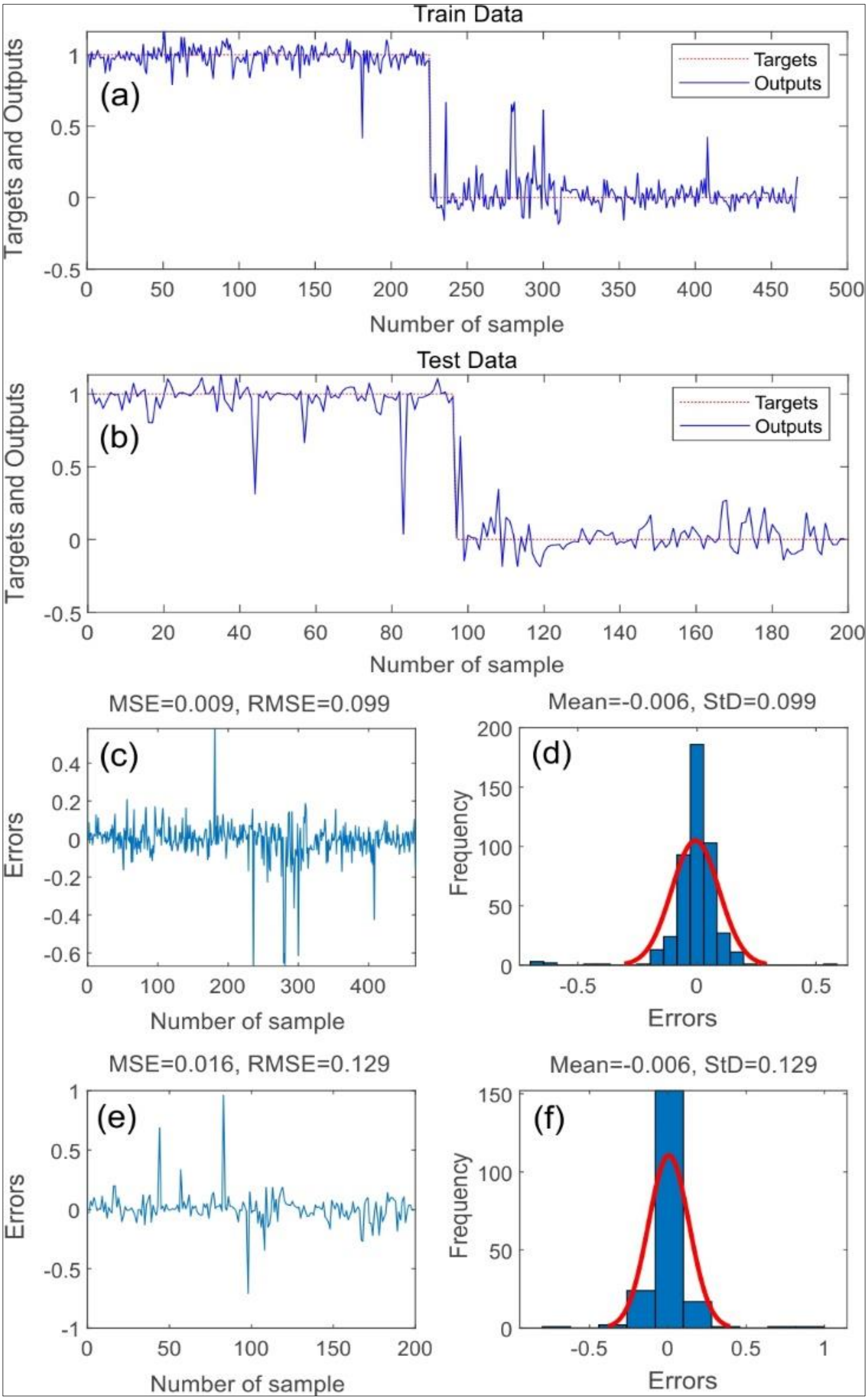

Fig. 10. GMDH-WOA performance: a) target and output values in the training phase, b) target and output values in the validation phase, c) magnitude of training error, d) distribution of training error, e) magnitude of validation error, and f) distribution of validation error.

We computed the success rate and prediction rate as the global performance metrics that further demonstrated the superiority of the hybrid models that achieved the highest training performance (success rate ≅ 0.93) compared to the standalone GMDH model (success rate ≅ 0.85) (Fig. 11a). In terms of the predictive capability (i.e., prediction rate), the hybrid models with the AUC values of >0.90 significantly outperformed the standalone GMDH model that had AUC = 0.79 (Fig. 11b).

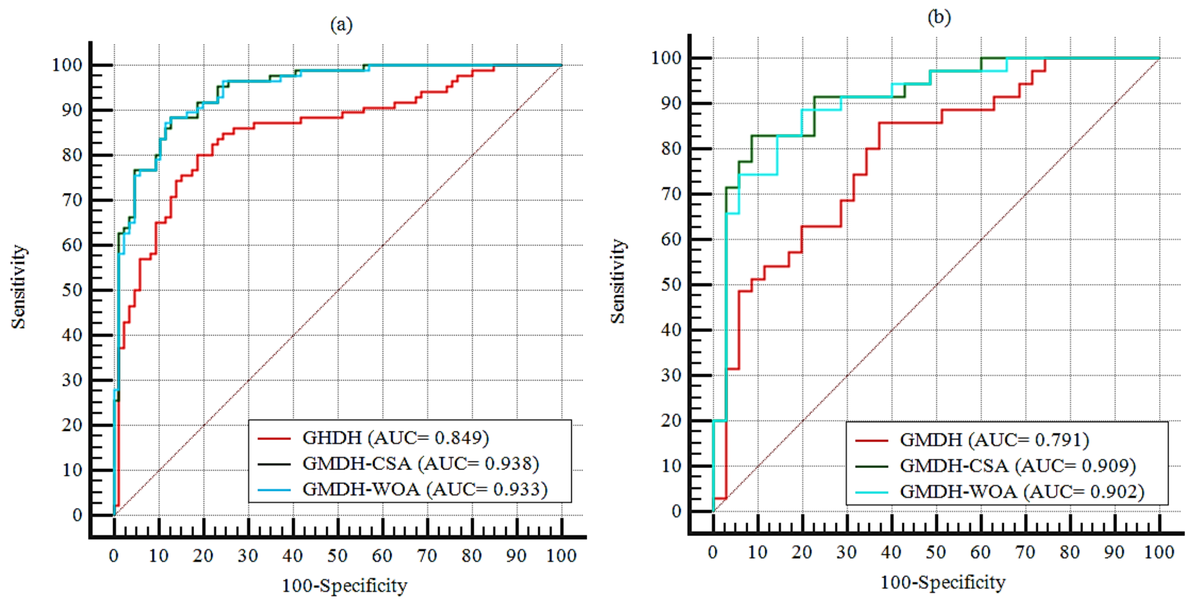

Fig. 11. (a) Success rates; and (b) prediction rates of the models

The Wilcoxon signed-rank test showed that except for the two hybrid models that were not significantly different from each other in both training (Table 2) and validation (Table 3) phases, *z*- and *p*-values for each of the other pair-wise comparisons of the three predictive models demonstrated that the generalization and predictive abilities of the standalone GMDH model are statistically significantly lower than the two hybrid models.

Table 2. Pairwise comparison of the success rates using the Wilcoxon signed-rank test.

Pair-wise comparison	Difference between AUCs	Standard error	95% confidence interval	*z*-value	*p*-value	Sig.
GMDH vs. GMDH-CSA	0.089	0.0168	0.0571 to 0.0123	5.366	0.0001	Yes
GMDH vs. GMDH-WOA	0.084	0.0168	0.0558 to 0.122	5.286	0.0001	Yes
GMDH-CSA vs. GMDH-WOA	0.005	0.00122	-0.00117 to 0.00360	1.000	0.3175	No

Table 3. Pair-wise comparison of the prediction rates using the Wilcoxon signed-rank test.

Pairwise comparison	Difference between AUCs	Standard error	95% confidence interval	*z*-value	*p*-value	Sig.
GMDH vs. GMDH-CSA	0.118	0.0295	0.0655 to 0.181	4.181	0.0001	Yes
GMDH vs. GMDH-WOA	0.111	0.0284	0.0594 to 0.171	4.053	0.0001	Yes
GMDH-CSA vs. GMDH-WOA	0.007	0.00643	-0.00444 to 0.0208	1.269	0.2043	No

The robustness analysis revealed that the standalone GMDH model performed slightly differently using different folds of training and validation datasets (Table 4). In the training phase, RMSEs and AUCs of the standalone GMDH model ranged from 0.224 to 0.235 (mean = 0.231), and from 0.841 to 0.849 (mean = 0.844), respectively. In the validation phase, RMSEs and AUCs of the standalone GMDH model ranged from 0.226 to 0.241 (mean = 0.235), and from 0.768 to 0.791 (mean = 0.779), respectively. However, the two hybrid models were stable when the datasets changed, indicating higher robustness compared to the standalone GMDH model.

Table 4. Robustness analysis using five-fold cross-validation.

Model	Phase	Measure	Fold 1	Fold 2	Fold 3	Fold 4	Fold 5	Mean
GMDH	Training	RMSE	0.224	0.231	0.231	0.235	0.235	0.231
		AUC	0.849	0.841	0.843	0.843	0.844	0.844
	Validation	RMSE	0.226	0.234	0.235	0.241	0.239	0.235
		AUC	0.791	0.777	0.784	0.768	0.774	0.779
GMDH-CSA	Training	RMSE	0.088	0.089	0.089	0.088	0.088	0.0884
		AUC	0.938	0.938	0.937	0.937	0.937	0.937
	Validation	RMSE	0.089	0.089	0.089	0.089	0.089	0.089
		AUC	0.909	0.909	0.909	0.909	0.909	0.909
GMDH-WOA	Training	RMSE	0.099	0.099	0.102	0.103	0.099	0.1004
		AUC	0.933	0.933	0.933	0.933	0.933	0.933
	Validation	RMSE	0.129	0.130	0.130	0.129	0.129	0.129
		AUC	0.902	0.902	0.902	0.902	0.902	0.902

4.3. Susceptibility maps

The landslide susceptibility values obtained from the application of three predictive models were used to develop the distribution maps of the landslide susceptibilities that were subsequently categorized into five (i.e., very low, low, moderate, high, and very high) susceptibility classes (Fig. 12). Whereas the hybrid GMDH-CSA and GMDH-WOA models revealed a relatively similar spatial variability of landslide susceptibilities across the study area, the standalone GMDH model produced a distribution map with greater portions of high and very high susceptibilities to landslide occurrences. In general, the south, southwestern, and central parts of the area are highly prone to landslide occurrences, while the northern and southwestern parts show significantly less landslide activity and are a rather low-susceptible zone. Visual comparison of the enlarged insets clipped from the susceptibility maps further revealed that susceptibility classes delineated by the standalone GMDH model disagreed with those defined by the hybrid models, particularly in areas without any evidence of historical landslides. The hybrid models generated a clearer and more accurate differentiation of zones with and without landslide, which is evident in the proportional distribution of the susceptibility classes each model assigned (Fig. 13). The standalone GMDH model has classified approximately 41% of the study area as highly landslide active, which contradicts the historical evidence of landslide occurrences in the area. Conversely, the hybrid models present more realistic representations of landslide susceptibility because the zones classified as high and very high susceptibility by these two models are smaller proportions of the whole.

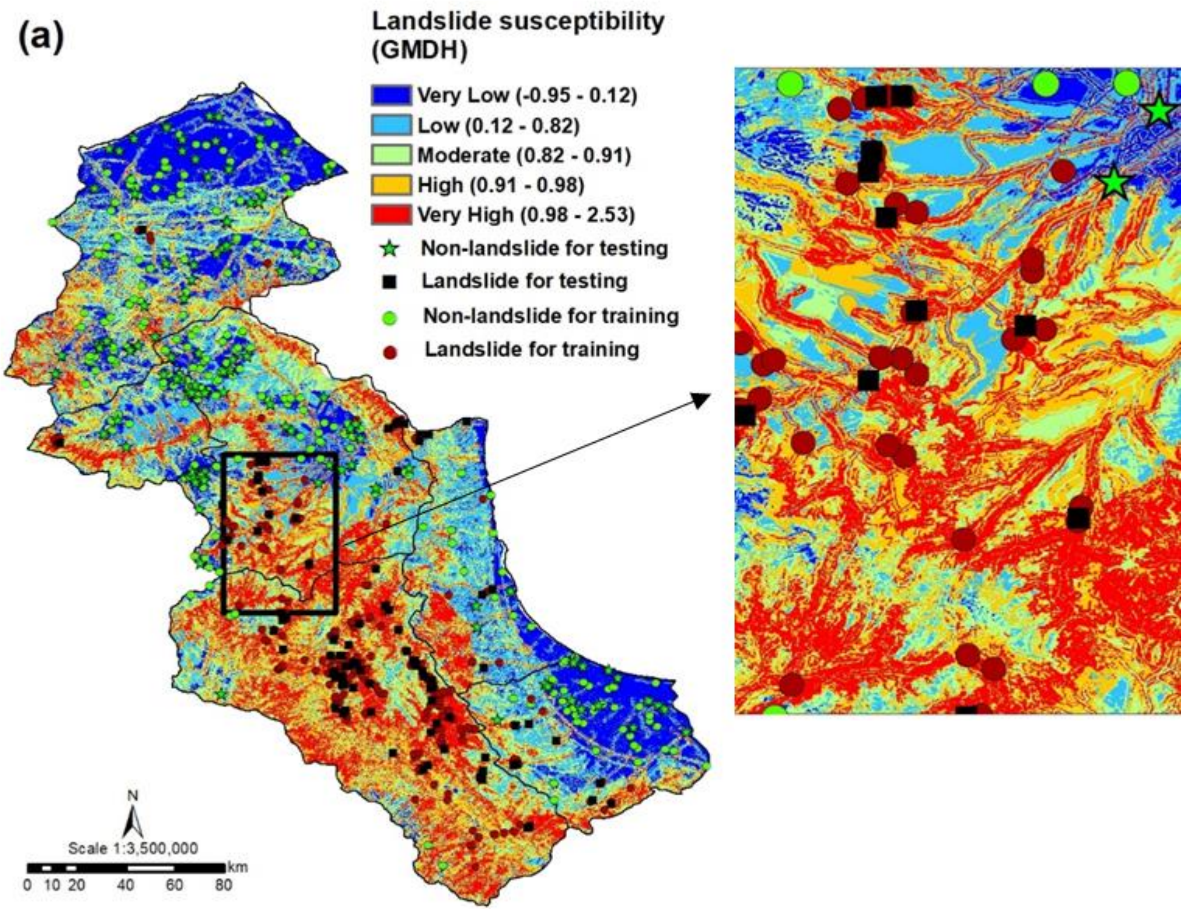

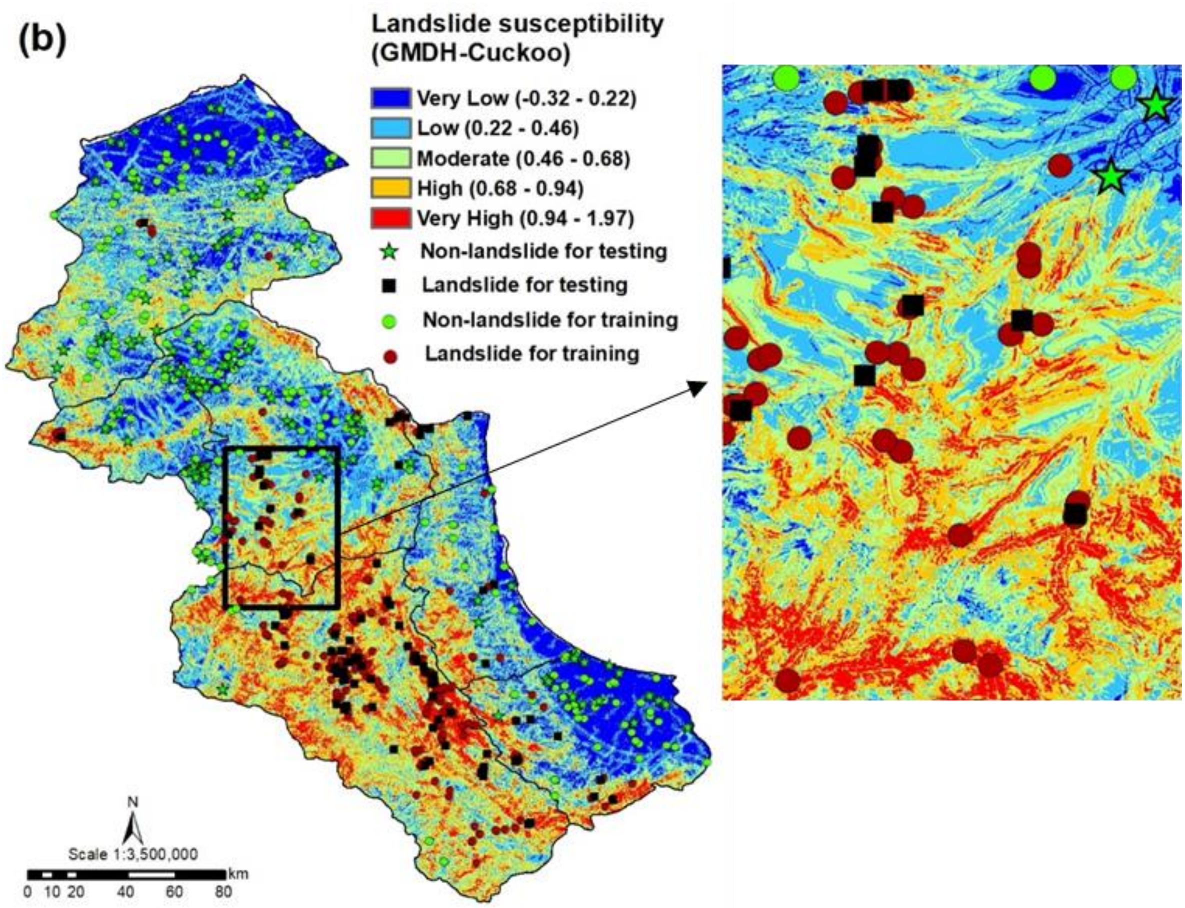

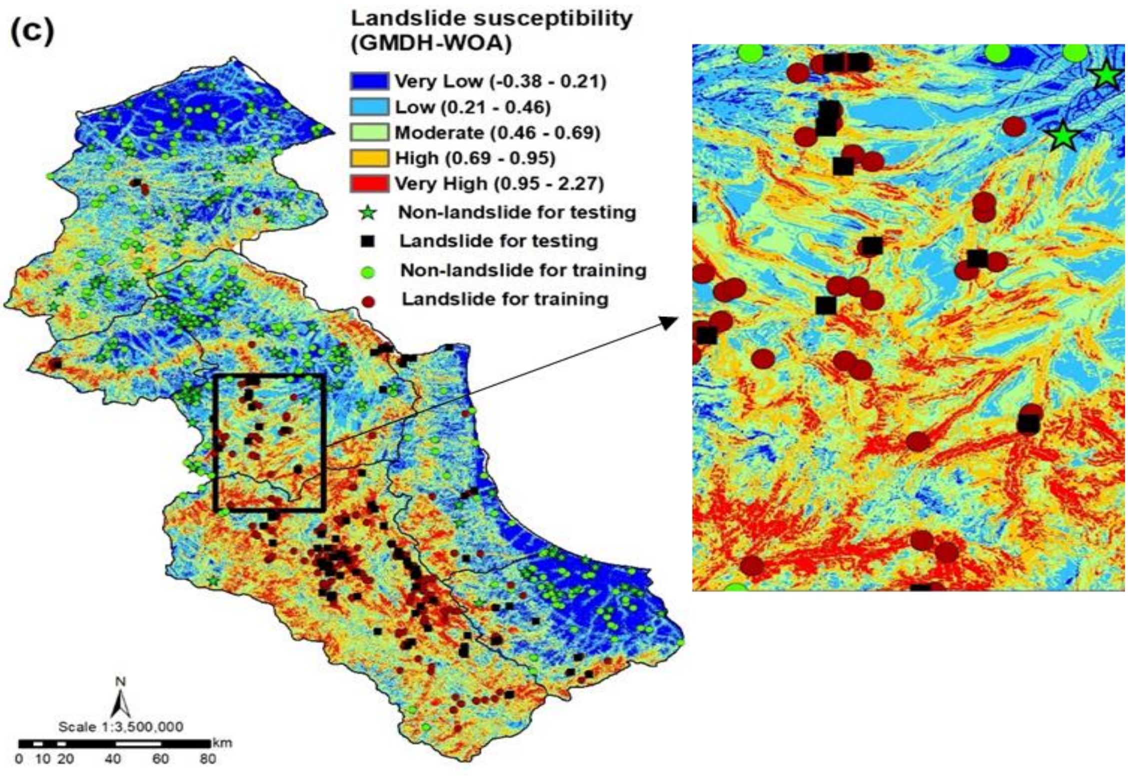

Fig. 12. Landslide susceptibility maps produced using the a) GMDH, b) GMDH-CSA, and c) GMDH-WOA models.

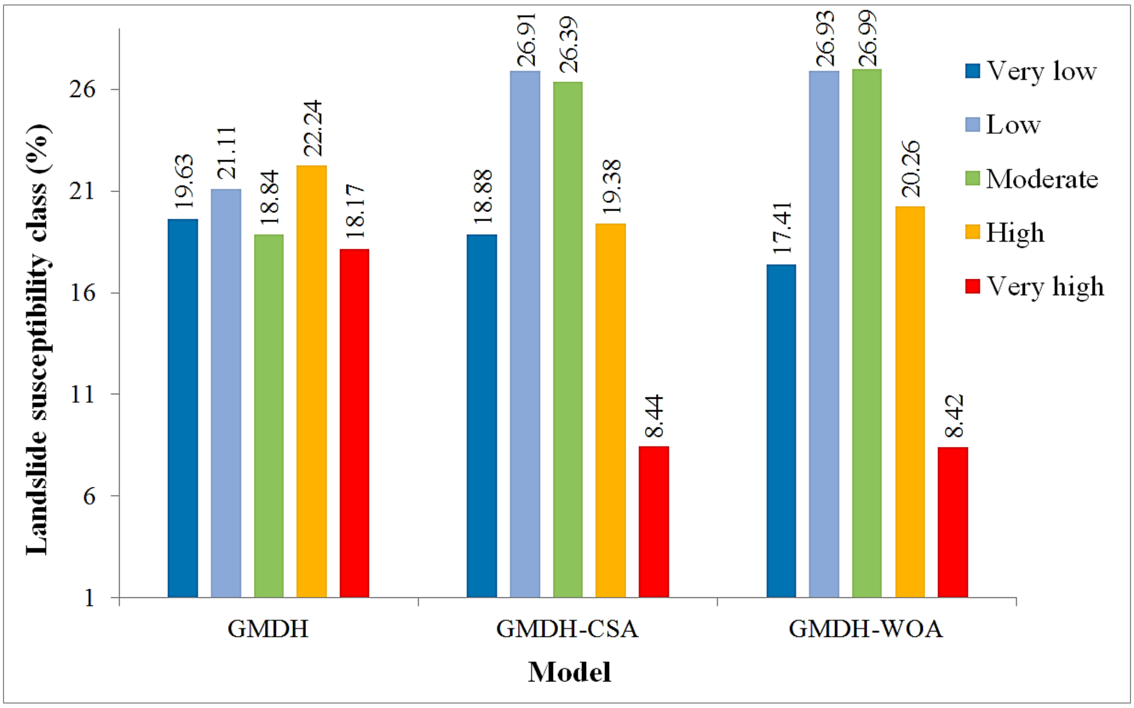

Fig. 13. Distribution of susceptibility classes in three landslide susceptibility maps.

5. Discussion

Landslides are dangerous hazards that seriously affect social life, economy, and environment. In this study, we developed two novel hybrid models that combine the GMDH method and the CSA and WOA optimization algorithms for the spatially explicit prediction of the landslide susceptibility. To the best of our knowledge, this is the first study that developed such predictive models and verified their utility using real-world data from a landslide-prone area. The recent works reported in the literature underscore the efficacy of swarm intelligence optimization algorithms for many real-world problems (Banadkooki et al., 2020; Jaafari et al., 2019b; Naghibi et al., 2017; Nguyen et al., 2019a). This greatly motivated us to utilize these two algorithms to optimize the GMDH model and develop two novel hybrid intelligence predictive models. These hybrid models allowed for spatially explicit predictions of future landslides based on the different geo-environmental factors that reflected local characteristics of the study area and the inherent behavior of historical landslides. Using a five-fold cross-validation procedure, the hybrid models achieved an average success rate of AUC = 0.935 compared to AUC = 0.844 achieved by the standalone GMDH model. In terms of the prediction rates, the average AUC values of 0.906 and 0.779 were produced by the hybrid models and standalone model, respectively. Higher success rate compared to the prediction rate is common, and generally expected since the models have been trained on a much larger data sample (70%) compared to the validation dataset (30%) (Rahmati et al., 2020). However, the standalone GMDH model showed a much greater AUC decreases from success rate to prediction rate compared to the hybrid models that indicate lower robustness and reliability. This problem can be attributed to the over-fitting during the training phase, in which the standalone GMDH model mostly describe the random patterns among the training data rather than learning to generalize from the relationships between the causative factors and historical landslides to predict future landslides (Jaafari et al., 2019b; Moayedi et al., 2019e; Rahmati et al., 2019b). The over-fitting problem can significantly decrease the generalization power and the transferability of the model outputs (Rahmati et al., 2020). A review of the literature reveals numerous examples of over-fitted and unreliable prediction outcomes due to the application of a single machine learning method alone (Bui et al., 2019; Liu et al., 2019; Nguyen et al., 2019b; Xi et al., 2019).

The robust and excellent predictive performance of our hybrid GMDH-CSA and GMDH-WOA models is indebted to a well-mapped of the historical landslides within the study area, selecting the most contributing causative factors that best defined the occurrence mechanism, and strength of the optimization algorithms (Liu et al., 2019; Moayedi et al., 2019b; Rahmati et al., 2019b; Tien Bui et al., 2019) that best adjusted the base GMDH model.

The AUC values of ≥0.90 for our novel models favorably fall within the range of the excellent predictive performances classified by Hosmer Jr et al. (2013) and the AUCs reported for the most recent intelligence hybrid models for the prediction of landslides around the world. For example, our hybrid models are quite competitive to the hybrid ANFIS-DE (AUC = 0.84), ANFIS-GA (AUC = 0.8), ANFIS-PSO (AUC = 0.78) models for the prediction of landslides in the Hanyuan County of China (Chen et al., 2017), to the hybrid SVM-ABC model (AUC = 0.90) for the prediction of landslides in the Lao Cai area in Vietnam (Bui et al., 2017), to the hybrid ANFIS-WOA (AUC = 0.86) and ANFIS-GWO (AUC = 0.87) models for the prediction of landslides in the Anyuan County of China (Chen et al., 2019a), and to the hybrid ANFIS-PSO (AUC =0.89) and ANFIS-SFLA (AUC = 0.89) models for the prediction of landslides in the Langao Hanyuan County of China (Chen et al., 2019b). However, our models were outperformed by the hybrid models developed by Jaafari et al. (2019a) that combined ANFIS with the GWO and BBO optimization algorithms (AUC ≅ 0.95) for the prediction of landslides in the Tehri Garhwal district of India, and Yuan and Moayedi (2019) who developed five hybrid models combining multilayer perceptron ANN (MLPANN) and ACO, PSO, GA, probability-based incremental learning (PBIL), and evolutionary strategy (ES) optimization algorithms and achieved AUCs ranging from 0.798 (ACO-MLPANN) to 0.960 (GA-MLPANN). These different model performances typically stem from three main sources. First, local characteristics of the research area and the situations that caused the landslides. Second, the size and quality of input data. In general, there is always a trade-off between the quality and size of the data utilized and the quality of modeling output (Jaafari, 2018; Jaafari et al., 2018; Moghaddam et al., 2020; Rahmati et al., 2019a). Lastly, the nature and proper configuration of the optimization algorithms (Bezerra et al., 2020) that were used to optimize the base model.

6. Conclusion

Despite the long-standing practice of landslide modeling and mapping, yet there is a need to enhance landslide prediction capabilities. Here, we approached this problem by developing two novel hybrid predictive models that combine the GMDH method with two meta-heuristic optimization algorithms. A spatially explicit database was used where a cross-validation procedure generated five different training and validation sets for handling uncertainty in data. Linking the historical landslides to a set of geo-environmental factors using two hybrid HDGH-CSA and GMDH-WOA models and the standalone GMDH model provided a reliable estimation of landslide susceptibility in a 31,340 Km^2 landscape in the northwest of Iran. Our hybrid models that profited from an intelligent approach to automatically adjust the parameters of the base GMDH model showed excellent performance in both training and validation phases, particularly when compared to the most recent proposed hybrid models for landslide prediction. In addition to the improved accuracy, our hybrid models demonstrated robust capacity to spatially explicit model landslide susceptibility. Looking forward, future works might incorporate other meta-heuristic optimization algorithms into the scheme. Such models can take manifold data from different sources into account to generate accurate estimates of landslide susceptibility even for complex terrains. These sophisticated predictive models are also applicable for the prediction of other types of natural hazards, such as floods, wildfires, land subsidence, and gully erosion, for the benefit of developing more efficient policies for the management of natural hazards.

References

Althuwaynee, O.F., Pradhan, B., Lee, S., 2012. Application of an evidential belief function model in landslide susceptibility mapping. Computers & Geosciences, 44, 120-135.

Banadkooki, F.B. et al., 2020. Enhancement of Groundwater-Level Prediction Using an Integrated Machine Learning Model Optimized by Whale Algorithm. Natural Resources Research, 1-20.

Bennett, N.D. et al., 2013. Characterising performance of environmental models. Environmental Modelling & Software, 40, 1-20.

Bezerra, L.C., López-Ibáñez, M., Stützle, T., 2020. Automatic configuration of multi-objective optimizers and multi-objective configuration, High-Performance Simulation-Based Optimization. Springer, pp. 69-92.

Brabb, E.E., Pampeyan, E.H., Bonilla, M.G., 1972. Landslide susceptibility in San Mateo County, California, US Geological Survey.

Bragagnolo, L., da Silva, R., Grzybowski, J., 2020a. Artificial neural network ensembles applied to the mapping of landslide susceptibility. Catena, 184, 104240.

Bragagnolo, L., da Silva, R.V., Grzybowski, J.M.V., 2020b. Landslide susceptibility mapping with r.landslide: A free open-source GIS-integrated tool based on Artificial Neural Networks. Environmental Modelling & Software, 123, 104565.

Bui, D.T. et al., 2019. Harris Hawks Optimization: A Novel Swarm Intelligence Technique for Spatial Assessment of Landslide Susceptibility. Sensors, 19, 3590.

Bui, D.T. et al., 2018. A novel integrated approach of Relevance Vector Machine optimized by imperialist competitive algorithm for spatial modeling of shallow landslides. Remote Sensing, 10.

Bui, D.T. et al., 2017. Spatial prediction of rainfall-induced landslides for the Lao Cai area (Vietnam) using a hybrid intelligent approach of least squares support vector machines inference model and artificial bee colony optimization. Landslides, 14, 447-458.

Carrara, A., Merenda, L., 1976. Landslide inventory in northern Calabria, southern Italy. Geological Society of America Bulletin, 87, 1153-1162.

Chen, W. et al., 2019a. Spatial Prediction of Landslide Susceptibility Using GIS-Based Data Mining Techniques of ANFIS with Whale Optimization Algorithm (WOA) and Grey Wolf Optimizer (GWO). Applied Sciences, 9, 3755.

Chen, W., Panahi, M., Pourghasemi, H.R., 2017. Performance evaluation of GIS-based new ensemble data mining techniques of adaptive neuro-fuzzy inference system (ANFIS) with genetic algorithm (GA), differential evolution (DE), and particle swarm optimization (PSO) for landslide spatial modelling. Catena, 157, 310-324.

Chen, W. et al., 2019b. Applying population-based evolutionary algorithms and a neuro-fuzzy system for modeling landslide susceptibility. Catena, 172, 212-231.

Dao, D.V. et al., 2020. A spatially explicit deep learning neural network model for the prediction of landslide susceptibility. CATENA, 188, 104451.

Dou, J. et al., 2019. Improved landslide assessment using support vector machine with bagging, boosting, and stacking ensemble machine learning framework in a mountainous watershed, Japan. Landslides, 1-18.

Du, J., Glade, T., Woldai, T., Chai, B., Zeng, B., 2020. Landslide susceptibility assessment based on an incomplete landslide inventory in the Jilong Valley, Tibet, Chinese Himalayas. Engineering Geology, 270, 105572.

EOS, N.s., 2017. A Global View of Landslide Susceptibility. https://earthobservatory.nasa.gov/images/89937/a-global-view-of-landslide-susceptibility, Access Data: April 15, 2020.

Fallah-Zazuli, M., Vafaeinejad, A., Alesheykh, A.A., Modiri, M., Aghamohammadi, H., 2019. Mapping landslide susceptibility in the Zagros Mountains, Iran: a comparative study of different data mining models. Earth Science Informatics, 12, 615-628.

Gascón-Moreno, J., Salcedo-Sanz, S., Saavedra-Moreno, B., Carro-Calvo, L., Portilla-Figueras, A., 2013. An evolutionary-based hyper-heuristic approach for optimal construction of group method of data handling networks. Information Sciences, 247, 94-108.

Glade, T., 2003. Landslide occurrence as a response to land use change: a review of evidence from New Zealand. Catena, 51, 297-314.

Gorum, T., Carranza, E., 2015. Control of style-of-faulting on spatial pattern of earthquake-triggered landslides. International journal of environmental science and technology, 12, 3189-3212.

Gorum, T., Gonencgil, B., Gokceoglu, C., Nefeslioglu, H., 2008. Implementation of reconstructed geomorphologic units in landslide susceptibility mapping: the Melen Gorge (NW Turkey). Natural Hazards, 46, 323-351.

Guzzetti, F., Carrara, A., Cardinali, M., Reichenbach, P., 1999. Landslide hazard evaluation: a review of current techniques and their application in a multi-scale study, Central Italy. Geomorphology, 31, 181-216.

Haklı, H., Uğuz, H., 2014. A novel particle swarm optimization algorithm with Levy flight. Applied Soft Computing, 23, 333-345.

Hanley, J.A., McNeil, B.J., 1982. The meaning and use of the area under a receiver operating characteristic (ROC) curve. Radiology, 143, 29-36.

Haque, U. et al., 2019. The human cost of global warming: deadly landslides and their triggers (1995–2014). Science of the total environment, 682, 673-684.

Harandizadeh, H., Armaghani, D.J., Khari, M., 2019. A new development of ANFIS–GMDH optimized by PSO to predict pile bearing capacity based on experimental datasets. Engineering with Computers, 1-16.

Highland, L., Bobrowsky, P.T., 2008. The landslide handbook: a guide to understanding landslides. US Geological Survey Reston.
Hong, H., Jaafari, A., Zenner, E.K., 2019. Predicting spatial patterns of wildfire susceptibility in the Huichang County, China: An integrated model to analysis of landscape indicators. Ecological Indicators, 101, 878-891.
Hosmer Jr, D.W., Lemeshow, S., Sturdivant, R.X., 2013. Applied logistic regression. John Wiley & Sons.
Ivakhnenko, A.G., 1968. The group method of data of handling; a rival of the method of stochastic approximation. Soviet Automatic Control, 13, 43-55.
Ivakhnenko, A.G., 1971. Polynomial theory of complex systems. IEEE transactions on Systems, Man, and Cybernetics, 364-378.
Jaafari, A., 2018. LiDAR-supported prediction of slope failures using an integrated ensemble weights-of-evidence and analytical hierarchy process. Environmental Earth Sciences, 77.
Jaafari, A., Gholami, D.M., Zenner, E.K., 2017. A Bayesian modeling of wildfire probability in the Zagros Mountains, Iran. Ecological Informatics, 39, 32-44.
Jaafari, A., Najafi, A., Pourghasemi, H.R., Rezaeian, J., Sattarian, A., 2014. GIS-based frequency ratio and index of entropy models for landslide susceptibility assessment in the Caspian forest, northern Iran. International Journal of Environmental Science and Technology, 11, 909-926.
Jaafari, A., Najafi, A., Rezaeian, J., Sattarian, A., 2015a. Modeling erosion and sediment delivery from unpaved roads in the north mountainous forest of Iran. GEM - International Journal on Geomathematics, 6, 343-356.
Jaafari, A., Najafi, A., Rezaeian, J., Sattarian, A., Ghajar, I., 2015b. Planning road networks in landslide-prone areas: A case study from the northern forests of Iran. Land Use Policy, 47, 198-208.
Jaafari, A. et al., 2019a. Meta optimization of an adaptive neuro-fuzzy inference system with grey wolf optimizer and biogeography-based optimization algorithms for spatial prediction of landslide susceptibility. Catena, 175, 430-445.
Jaafari, A., Razavi Termeh, S.V., Bui, D.T., 2019b. Genetic and firefly metaheuristic algorithms for an optimized neuro-fuzzy prediction modeling of wildfire probability. Journal of Environmental Management, 243, 358-369.
Jaafari, A., Zenner, E.K., Panahi, M., Shahabi, H., 2019c. Hybrid artificial intelligence models based on a neuro-fuzzy system and metaheuristic optimization algorithms for spatial prediction of wildfire probability. Agricultural and Forest Meteorology, 266-267, 198-207.
Jaafari, A., Zenner, E.K., Pham, B.T., 2018. Wildfire spatial pattern analysis in the Zagros Mountains, Iran: A comparative study of decision tree based classifiers. Ecological Informatics, 43, 200-211.
Jessee, M.A.N., Hamburger, M., Ferrara, M., McLean, A., FitzGerald, C., 2020. A global dataset and model of earthquake-induced landslide fatalities. Landslides, 1-14.
Larsen, I.J., Montgomery, D.R., 2012. Landslide erosion coupled to tectonics and river incision. Nature Geoscience, 5, 468-473.
Liu, L., Moayedi, H., Rashid, A.S.A., Rahman, S.S.A., Nguyen, H., 2019. Optimizing an ANN model with genetic algorithm (GA) predicting load-settlement behaviours of eco-friendly raft-pile foundation (ERP) system. Engineering with Computers, 35, 1-13.
Machado, R.A., Oliveira, A.G., Lois-González, R.C., 2019. Urban ecological infrastructure: The importance of vegetation cover in the control of floods and landslides in Salvador/Bahia, Brazil. Land Use Policy, 89, 104180.
Mafi-Gholami, D., Zenner, E.K., Jaafari, A., 2020. Mangrove regional feedback to sea level rise and drought intensity at the end of the 21st century. Ecological Indicators, 110, 105972.
Mafi-Gholami, D., Zenner, E.K., Jaafari, A., Ward, R.D., 2019. Modeling multi-decadal mangrove leaf area index in response to drought along the semi-arid southern coasts of Iran. Science of the Total Environment, 656, 1326-1336.
Meneses, A.A.d.M., da Silva, P.V., Nast, F.N., Araujo, L.M., Schirru, R., 2020. Application of Cuckoo Search algorithm to Loading Pattern Optimization problems. Annals of Nuclear Energy, 139, 107214.
Mirjalili, S., Lewis, A., 2016. The Whale Optimization Algorithm. Advances in Engineering Software, 95, 51-67.

Moayedi, H. et al., 2019a. Novel hybrids of adaptive neuro-fuzzy inference system (ANFIS) with several metaheuristic algorithms for spatial susceptibility assessment of seismic-induced landslide. Geomatics, Natural Hazards and Risk, 10, 1879-1911.

Moayedi, H., Nguyen, H., Rashid, A.S.A., 2019b. Comparison of dragonfly algorithm and Harris hawks optimization evolutionary data mining techniques for the assessment of bearing capacity of footings over two-layer foundation soils. Engineering with Computers, 1-11.

Moayedi, H. et al., 2019c. Two novel neural-evolutionary predictive techniques of dragonfly algorithm (DA) and biogeography-based optimization (BBO) for landslide susceptibility analysis. Geomatics, Natural Hazards and Risk, 10, 2429-2453.

Moayedi, H., Osouli, A., Tien Bui, D., Foong, L.K., 2019d. Spatial Landslide Susceptibility Assessment Based on Novel Neural-Metaheuristic Geographic Information System Based Ensembles. Sensors, 19, 4698.

Moayedi, H., Tien Bui, D., Gör, M., Pradhan, B., Jaafari, A., 2019e. The feasibility of three prediction techniques of the artificial neural network, adaptive neuro-fuzzy inference system, and hybrid particle swarm optimization for assessing the safety factor of cohesive slopes. ISPRS International Journal of Geo-Information, 8, 391.

Moghaddam, D.D. et al., 2020. The effect of sample size on different machine learning models for groundwater potential mapping in mountain bedrock aquifers. CATENA, 187, 104421.

Naghibi, S.A., Ahmadi, K., Daneshi, A., 2017. Application of Support Vector Machine, Random Forest, and Genetic Algorithm Optimized Random Forest Models in Groundwater Potential Mapping. Water Resources Management, 31, 2761-2775.

Nefeslioglu, H.A., Gorum, T., 2020. The use of landslide hazard maps to determine mitigation priorities in a dam reservoir and its protection area. Land Use Policy, 91, 104363.

Nguyen, H., Mehrabi, M., Kalantar, B., Moayedi, H., Abdullahi, M.a.M., 2019a. Potential of hybrid evolutionary approaches for assessment of geo-hazard landslide susceptibility mapping. Geomatics, Natural Hazards and Risk, 10, 1667-1693.

Nguyen, H. et al., 2019b. Optimizing ANN models with PSO for predicting short building seismic response. Engineering with Computers, 35, 1-15.

Nhu, V.-H. et al., 2020. GIS-Based Gully Erosion Susceptibility Mapping: A Comparison of Computational Ensemble Data Mining Models. Applied Sciences, 10, 2039.

Petrović, M., Miljković, Z., Jokić, A., 2019. A novel methodology for optimal single mobile robot scheduling using whale optimization algorithm. Applied Soft Computing, 81, 105520.

Pham, B.T. et al., 2019. Hybrid computational intelligence models for groundwater potential mapping. Catena, 182.

Pourghasemi, H.R., Rahmati, O., 2018. Prediction of the landslide susceptibility: Which algorithm, which precision? Catena, 162, 177-192.

Rahmati, O. et al., 2019a. PMT: New analytical framework for automated evaluation of geo-environmental modelling approaches. Science of the Total Environment, 664, 296-311.

Rahmati, O. et al., 2020. Hybridized neural fuzzy ensembles for dust source modeling and prediction. Atmospheric Environment, 224, 117320.

Rahmati, O. et al., 2019b. Capability and robustness of novel hybridized models used for drought hazard modeling in southeast Queensland, Australia. Science of The Total Environment, 134656.

Reichenbach, P., Mondini, A., Rossi, M., 2014. The influence of land use change on landslide susceptibility zonation: the Briga catchment test site (Messina, Italy). Environmental management, 54, 1372-1384.

Saberi-Movahed, F., Najafzadeh, M., Mehrpooya, A., 2020. Receiving More Accurate Predictions for Longitudinal Dispersion Coefficients in Water Pipelines: Training Group Method of Data Handling Using Extreme Learning Machine Conceptions. Water Resources Management, 34, 529-561.

Sanajaoba, S., Fernandez, E., 2016. Maiden application of Cuckoo Search algorithm for optimal sizing of a remote hybrid renewable energy System. Renewable Energy, 96, 1-10.

Schlögl, M., Matulla, C., 2018. Potential future exposure of European land transport infrastructure to rainfall-induced landslides throughout the 21st century. Natural Hazards and Earth System Sciences, 18, 1121-1132.

Shafizadeh-Moghadam, H., Minaei, M., Shahabi, H., Hagenauer, J., 2019. Big data in Geohazard; pattern mining and large scale analysis of landslides in Iran. Earth Science Informatics, 12.

Shu, H. et al., 2019. Relation between land cover and landslide susceptibility in Val d'Aran, Pyrenees (Spain): Historical aspects, present situation and forward prediction. Science of the total environment, 693, 133557.

Thanh, D.Q. et al., 2020. GIS based frequency ratio method for landslide susceptibility mapping at Da Lat City, Lam Dong province, Vietnam. VIETNAM JOURNAL OF EARTH SCIENCES, 42, 55-66.

Tien Bui, D., Moayedi, H., Gör, M., Jaafari, A., Foong, L.K., 2019. Predicting slope stability failure through machine learning paradigms. ISPRS International Journal of Geo-Information, 8, 395.

Tosteson, A.N.A., Begg, C.B., 1988. A general regression methodology for ROC curve estimation. Medical Decision Making, 8, 204-215.

Van Westen, C., Rengers, N., Soeters, R., 2003. Use of geomorphological information in indirect landslide susceptibility assessment. Natural hazards, 30, 399-419.

Van Westen, C.J., Castellanos, E., Kuriakose, S.L., 2008. Spatial data for landslide susceptibility, hazard, and vulnerability assessment: an overview. Engineering geology, 102, 112-131.

Vanmaercke, M., Ardizzone, F., Rossi, M., Guzzetti, F., 2017. Exploring the effects of seismicity on landslides and catchment sediment yield: An Italian case study. Geomorphology, 278, 171-183.

Witczak, M., Korbicz, J., Mrugalski, M., Patton, R.J., 2006. A GMDH neural network-based approach to robust fault diagnosis: Application to the DAMADICS benchmark problem. Control Engineering Practice, 14, 671-683.

Wood, J.L., Harrison, S., Reinhardt, L., Taylor, F.E., 2020. Landslide databases for climate change detection and attribution. Geomorphology, 355, 107061.

Xi, W., Li, G., Moayedi, H., Nguyen, H., 2019. A particle-based optimization of artificial neural network for earthquake-induced landslide assessment in Ludian county, China. Geomatics, Natural Hazards and Risk, 10, 1750-1771.

Yang, X.-S., 2013. Cuckoo search and firefly algorithm: Theory and applications. Springer.

Yang, X.-S., 2014. Cuckoo search and firefly algorithm: overview and analysis, Cuckoo search and firefly algorithm. Springer, pp. 1-26.

Yang, X.-S., Deb, S., 2009. Cuckoo search via Lévy flights, 2009 World congress on nature & biologically inspired computing (NaBIC). IEEE, pp. 210-214.

Yuan, C., Moayedi, H., 2019. Evaluation and comparison of the advanced metaheuristic and conventional machine learning methods for the prediction of landslide occurrence. Engineering with Computers, 1-11.